



LUND UNIVERSITY

Analytical and Numerical Developments in Strongly Correlated Systems: Perspectives from TDDFT and Green's Functions

Karlsson, Daniel

2014

Document Version:

Publisher's PDF, also known as Version of record

[Link to publication](#)

Citation for published version (APA):

Karlsson, D. (2014). *Analytical and Numerical Developments in Strongly Correlated Systems: Perspectives from TDDFT and Green's Functions*. [Doctoral Thesis (compilation), Mathematical Physics]. Division of Mathematical Physics, Faculty of Science, Lund University.

Total number of authors:

1

General rights

Unless other specific re-use rights are stated the following general rights apply:

Copyright and moral rights for the publications made accessible in the public portal are retained by the authors and/or other copyright owners and it is a condition of accessing publications that users recognise and abide by the legal requirements associated with these rights.

- Users may download and print one copy of any publication from the public portal for the purpose of private study or research.
- You may not further distribute the material or use it for any profit-making activity or commercial gain
- You may freely distribute the URL identifying the publication in the public portal

Read more about Creative commons licenses: <https://creativecommons.org/licenses/>

Take down policy

If you believe that this document breaches copyright please contact us providing details, and we will remove access to the work immediately and investigate your claim.

LUND UNIVERSITY

PO Box 117
221 00 Lund
+46 46-222 00 00

ANALYTICAL AND NUMERICAL DEVELOPMENTS IN
STRONGLY CORRELATED SYSTEMS:
PERSPECTIVES FROM TDDFT AND GREEN'S
FUNCTIONS

DANIEL KARLSSON



LUND
UNIVERSITY

DIVISION OF MATHEMATICAL PHYSICS
FACULTY OF SCIENCE

LUND UNIVERSITY 2014

© 2014 Daniel Karlsson

Paper I © 2011 by the European Physical Society

Paper II © 2011 by the American Physical Society

Paper III © 2013 by Nature Publishing Group

Paper IV © 2013 by the American Physical Society

Paper V © 2014 by the authors. Submitted to Physical Review Letters.

ISBN-978-91-7473-981-7 (print)

ISBN-978-91-7473-982-4 (pdf)

Lund-MPh-14/04

Printed in Sweden by Mediatryck, Lund 2014

ANALYTICAL AND NUMERICAL DEVELOPMENTS IN
STRONGLY CORRELATED SYSTEMS:
PERSPECTIVES FROM TDDFT AND GREEN'S
FUNCTIONS

DANIEL KARLSSON

DIVISION OF MATHEMATICAL PHYSICS
FACULTY OF SCIENCE
LUND UNIVERSITY, SWEDEN

DISSERTATION FOR THE DEGREE OF
DOCTOR OF PHILOSOPHY


THESIS ADVISOR:
ASS. PROF. CLAUDIO VERDOZZI

FACULTY OPPONENT:
PROF. ROBERT VAN LEEUWEN

ACADEMIC DISSERTATION WHICH, BY DUE PERMISSION OF THE FACULTY OF SCIENCE AT LUND
UNIVERSITY, WILL BE PUBLICLY DEFENDED ON WEDNESDAY, JUNE 4TH, 2014, AT 13.15 IN
RYDBERGSSALEN, SÖLVEGATAN 14A, LUND, FOR THE DEGREE OF DOCTOR OF PHILOSOPHY.

Organization LUND UNIVERSITY Department of Physics Division of Mathematical Physics Box 118, SE-22100 LUND, SWEDEN	Document name DOCTORAL DISSERTATION	
	Date of issue 2014-05-05	
Author(s) Daniel Karlsson	Sponsoring organization	
Title and subtitle Analytical and Numerical Developments in Strongly Correlated Systems: Perspectives from TDDFT and Green's Functions		
Abstract This thesis investigates different methods for treating strongly correlated systems, and discusses their respective strengths and weaknesses. Many of the results presented in this thesis come from comparing the different methods and approximations to exact results. Paper I: We studied the real-time dynamics of a trapped fermion gas, as it expands after removal of a trapping potential. Paper II: We constructed a new exchange-correlation potential, to be used in three dimensions. The potential is non-perturbative in the interaction, meaning that we could use it both for weakly interacting (metallic) systems, as well as for strongly interacting (Mott insulating) systems. Paper III: We studied transport of electrons through small disordered wires contacted to leads. Using TDDFT, we have studied how the inclusion of both disorder and large electron-electron interactions affect conduction. At finite bias, we saw that the effects were competitive, and that interactions could increase the current through disordered samples. Paper IV: We studied fermions in 3D, using our newly developed exchange-correlation potentials, presented in Paper II. We studied how a cloud of fermions expands when released from a trapping potential. The simulated systems were large enough to be relevant for actual experimental conditions. Paper V: We studied transport of electrons through small disordered wires contacted to leads. The setup was similar to the one in Paper III, but another method was used - NEGF. Many of the observed trends were similar to those seen in our previous investigations. The differences were attributed to non-local effects.		
Key words Green's function, DFT, TDDFT, Hubbard model, Many-Body Perturbation Theory, Quantum Transport, Disorder		
Classification system and/or index terms (if any)		
Supplementary bibliographical information		Language English
ISSN and key title		ISBN 978-91-7473-981-7
Recipient's notes	Number of pages	Price
	Security classification	

Distribution by Daniel Karlsson, Division of Mathematical Physics, Lund University, Box 118, SE-22100 LUND
I, the undersigned, being the copyright owner of the abstract of the above-mentioned dissertation, hereby grant to all reference sources permission to publish and disseminate the abstract of the above-mentioned dissertation.

Signature 

Date 2014-05-05

Summary of the papers

Paper I

Dynamical self-stabilization of the Mott insulator: Time evolution of the density and entanglement entropy of out-of-equilibrium cold fermion gases.

Daniel Karlsson, Claudio Verdozzi, Mariana. M. Odashima, and Klaus Capelle
EPL, **93** 23003, (2011)

In this work we have studied theoretically the real-time dynamics of a trapped fermion gas, as it expands upon the removal of the trapping potential. By choosing the parameters such that the system is strongly interacting, we were able to study the dynamics of several different local phases: metallic, Mott insulating and band insulating phases. We showed that the Mott insulating and band insulating phase have drastically different behaviours. The band insulator melted in a short time frame, while the Mott insulator was extremely stable, in comparison. We also introduced an ALDA for the entanglement entropy, a quantity which contains information about phase transitions, and showed that in the ALDA we can also see local phase transitions in the time-dependent entanglement entropy.

My contributions to the paper consisted of writing parts of the TDDFT code, running all calculations, discussing the results, and participating in writing the paper.

Paper II

Time-Dependent Density-Functional Theory Meets Dynamical Mean-Field Theory: Real-Time Dynamics for the 3D Hubbard Model

Daniel Karlsson, Antonio Privitera, and Claudio Verdozzi
Physical Review Letters, **106** 116401, (2011)

We have constructed a new exchange-correlation potential v_{xc} , to be used in three dimensions. In order to do this we solved the infinite homogeneous Hubbard model in 3D using the approximate method of Dynamical Mean Field Theory. By doing this, we could obtain a v_{xc} which is non-perturbative in the interaction, meaning that we could use it both for weakly interacting (metallic) systems as well as for strongly interacting (Mott insulating) systems. The new exchange-correlation potential was benchmarked in a test system against exact diagonalization, and was found to perform well in most scenarios. When the method seemed to fail, we showed that this was not due to DMFT, but instead to the Local Density Approximation itself. This points to the fact, at least in our test system, that the DMFT potential is a very good potential used in the LDA approximation.

My contributions to the paper consisted of writing parts of the TDDFT code, interpolating the ground state energy data obtained from DMFT. I performed a smoothening and fitting procedure of the data. I performed all the DFT and TDDFT calculations. I took part in the writing of the paper as well as discussion of the results.

Paper III

Interacting fermions in one-dimensional disordered lattices: Exploring localization and transport properties with lattice density-functional theories

Valeria Vettchinkina, Alexey Kartsev, Daniel Karlsson, and Claudio Verdozzi

Physical Review B, **87** 115117, (2013)

In this work we have studied the transport of electrons through small disordered wires, contacted to leads. Using TDDFT, we have studied how the inclusion of both disorder and large electron-electron interactions affects the conduction and localization of the electrons. At finite bias, we saw that the effects were competitive, and that interactions could increase the current through disordered samples.

My contributions to the paper consisted of developing scripts and code to do disorder averaging and post-processing, actively discussing the results, analysing the data, and participated in the writing of the paper.

Paper IV

Three-dimensional dynamics of a fermionic Mott wedding-cake in clean and disordered optical lattices

Alexey Kartsev, Daniel Karlsson, Antonio Privitera, and Claudio Verdozzi
Scientific Reports, **3** (2570):1–7, (2013)

In this work we studied fermions in 3D, using our newly developed exchange-correlation potential from DMFT, as done in Paper II. We studied how a cloud of fermions would expand, as they were released from a parabolic potential. These simulations were made large enough to be relevant to actual experimental conditions in the cold atom community, proving a point that it is indeed possible to simulate such large systems. In the results we could see similar trends that we saw in Paper I, that the Mott insulating region is quite stable to external perturbations. We could also see that the inclusion of disorder could destabilize the Mott region, making it melt more easily.

My contributions to the paper consisted of analyzing the results of the simulations, actively discussing the results, discussing the setup and strategy of the simulations, and participating in the writing of the paper.

Paper V

Transport of Correlated Electrons through Disordered Chains: A Perspective on Entanglement, Conductance, and Disorder Averaging

Daniel Karlsson and Claudio Verdozzi
arXiv:0970563

We investigate electron transport in disordered Hubbard chains contacted to macroscopic leads, via the non-equilibrium Green's functions technique. We observe a crossover of currents and conductances at finite bias which depends on the relative strength of disorder and interactions. The finite-size scaling of the conductance is highly dependent on the interaction strength, and exponential attenuation is not always seen. We provide a proof that the Coherent Potential Approximation, a widely used method for treating disorder averages, fulfils particle conservation at finite bias with or without electron correlations. Finally, our results hint that the observed trends in conductance due to interactions and disorder also appear as signatures in the single-site entanglement entropy.

My contributions to the paper consisted of coming up with some of the main ideas of the project, developing a steady-state Non-Equilibrium Green's Function code, making the simulations, analyzed the results and wrote the first draft of the paper.

Articles not included in the thesis

Paper VI

Some open questions in TDDFT: Clues from lattice models and Kadanoff-Baym dynamics

Claudio Verdozzi, Daniel Karlsson, Marc Puig von Friesen, Carl-Olof Almbladh, and Ulf von Barth

Chem. Phys. **391** 1 Pages 37–49 (2011)

Acknowledgements

The first time I met Claudio was in the spring of 2007. His passion for science and his ability to motivate and inspire opened my eyes for the wonders of solid state physics, as well as numerical methods and programming. He helped me find my position in the group and at the division of mathematical physics. Since then he has been my supervisor, and he has guided me through my time as a PhD student. I have learned so much from him during our years of working together. Claudio's specialty of finding alternative paths has been a great motivation, and has taught me that it is possible to turn apparent problems into scientific discoveries. Thank you.

I would also like to thank Carl-Olof and Ulf for welcoming me to the group, and always being willing to share your immense experience and wisdom with me. Moreover, you were the first ones to teach me about the world of quantum mechanics and solid state physics in my early courses at the university. My path would not have been the same without you.

During my years at the division, I have had the great pleasure of meeting many people. Some of you who I have worked with, have left the division and continued your careers elsewhere. Marc, thank you for patiently explaining your work to me during the short time we had together in the group. Alexey, thank you for the hard and devoted work you put into our joint projects. Valeria, thank you for all our enjoyable and enlightening hour-long discussions on various topics including physics concepts, lemon cakes, and life in general. It was great working together with all of you.

I am also grateful to the present people in the group, Emil and Miroslav. Having you around for discussions on physics and various other matters has been invaluable to me.

I would also like to thank everyone at the division, for providing a pleasant workplace where every lunch and 'fika' in the kitchen was an opportunity for fun discussions. A

special thanks goes to Katarina, for always taking care of confused physicists, and Elife, for being a provider of friendship and cookies. Thanks to my office mate Christian, for heated and educational discussions. Thanks to Sven, for all your efforts of making the division a pleasant environment to work in.

I would also like to thank my friends outside of the division. In particular, I would like to mention Nils and Maciek. Special thanks also go to my childhood friend Aidin, who keeps showing me that there is more to life than PhD work.

Tack till min familj, som alltid stöttar mig och låter mig gå min egen väg. Jag är glad att jag har er.

Tack Ulrika. Det hade inte gått utan dig.

Populär sammanfattning

Genom århundradena har ingenjörskonsten och naturvetenskapen genomsyrats av en önskan att förstå och kontrollera den materia som omger oss. All materia, till exempel träd, byggnader och mobiltelefoner, består av olika slags atomer som är arrangerade i en mängd olika strukturer. Från människans första försök att tillverka redskap genom att manipulera flintstenar och metaller, till dagens allestädes närvarande tekniska underverk, har förståelsen av materien gått hand i hand med möjligheten att kontrollera densamma.

På senare tid har forskare lärt sig att kontrollera enstaka molekylers position. På så vis kan man få molekyler att bilda kedjor vars tjocklek är av nanostorlek. Om en sådan kedja placeras mellan två elektriska kontakter, kan man få en ström att flyta genom den, precis som genom en vanlig kopparledning. Skillnaden är att när kedjan består av enstaka molekyler dyker en del nya och ibland oväntade fenomen upp. Istället för att resistansen i ledaren kan beräknas om man känner materialet, utformningen och temperaturen, såsom är fallet med vanliga sladdar, beror den nu på fler variabler. I sådana här nanosystem kan resistansen ändra sig språngvis, och plötsligt blir strömmen mycket större eller mycket mindre än vad man skulle förväntat sig.

Detta till synes märkliga beteende, som inte alls verkar överensstämma med det man observerar för vanliga sladdar, kommer sig av att vi kommer närmare materiens grundstenar. Egentligen betar sig allting omkring oss på det vis som beskrivs av den så kallade kvantmekaniken, men bara när vi studerar mycket speciella system kan vi observera den direkt. För makroskopiskt stora objekt, såsom kopparledningar, summeras de enskilda atomernas beteende och *i genomsnitt* betar de sig såsom vi är vana vid från århundraden av undersökningar. Upptäckten att en annan fysik behövs när man studerar enskilda atomer kom som en chock för forskarna för cirka hundra år sedan.

Kanske kan materiens detaljbeskrivning tyckas onödig, men faktiskt gör sig kvantmekanikens effekter påminna redan i de transistorer som används i dagens datorer. Kvantmekaniken behövs t.ex. för att förklara sprången i resistansen hos nanomaterial. Problemet är att det är mycket svårt att beräkna egenskaper hos material utifrån dessa grundläggande principer. Datorsimuleringar är ofta extremt svåra och tidskrävande. Ofta vet man inte heller exakt hur ens system ser ut, eftersom parametrar såsom renhet eller atomers exakta position är svåra att bestämma i de nanosystem som man framställer experimentellt.

Därför krävs ett annorlunda angreppssätt för att lära känna dessa små men extremt intressanta objekt. I denna avhandling beskriver jag mina försök att göra kvantmekaniska beräkningar genom att förenkla verkligheten till modeller. De modeller jag använder saknar viss information och ignorerar vissa effekter som finns i riktig materia, men de kan ändå användas för att i detalj studera specifika delar av kvantmekanikens uttryck. Genom att skilja ut vissa delar av verkligheten kan man lära sig mer om just dem utan att behöva göra bilden överdrivet komplicerad och så detaljrik att man inte ser skogen för alla träd.

När man förstår de olika delarna kan man sedan lägga samman kunskapen till en mer komplett beskrivning av materien. Man kan också, när man lärt sig tillräckligt om den viss del, förenkla beskrivningen och därmed också göra beräkningar snabbare. Det finns också situationer där vissa effekter är mycket viktigare än andra. Detta gör att den förenklade modellen i sig kan beskriva allt väsentligt. Dessutom kan man genom att undersöka en modell kanske slå fast att en effekt *inte* behövs för en viss situation, och då kan man bortse från den, och ändå få en fullständig beskrivning.

Som ett exempel från den klassiska mekaniken, kan man nämna att fysiker ofta förenklar sin beskrivning av världen genom att anta att det inte finns något luftmotstånd. När de tidiga fysikerna testade vad som hände genom att låta saker falla i vacuum, förstod de mer om hur gravitation fungerar. Genom att undersöka olika delar av verkligheten var för sig, blev det lättare att förstå gravitation, och lättare att förstå luftmotstånd. När man sedan har förstått fenomenen är det lättare att för varje situation man vill beskriva se om luftmotståndet är försumbart eller måste tas i beaktan.

På detta sätt hoppas jag att resultaten av min forskning kommer att bidra till förståelsen av världen omkring oss, och samtidigt ge oss möjlighet att kontrollera den

ännu bättre. Exakt vad mina modeller och beräkningar leder till går inte att säga idag. Mycket av dagens teknik skulle man inte ha kunnat föreställa sig för hundra år sedan. Vanligtvis föreställer man sig att dagens teknik i framtiden kommer ha förfinats till perfektion. Det är betydligt svårare att tänka sig de helt nya saker som uppstår då förståelsen av omvärlden och möjligheten att kontrollera den tar ett stort kliv framåt, såsom till exempel när elektriciteten upptäcktes och togs i människans tjänst. Detta är charmen med grundforskning - den leder till genombrott man idag inte ens kan föreställa sig.

Acronyms

DFT Density Functional Theory

TDDFT Time-Dependent Density Functional Theory

DMFT Dynamical Mean-Field Theory

LDA Local Density Approximation

ALDA Adiabatic Local Density Approximation

BALDA Bethe-Ansatz Local Density Approximation

KS Kohn-Sham

HF Hartree-Fock

NEGF Non-Equilibrium Green's function

CPA Coherent Potential Approximation

IPR Inverse Participation Ratio

Contents

1	Introduction	1
2	Theory	5
2.1	The Model	5
2.2	Density Functional Theory (DFT)	8
2.3	Time-Dependent Density Functional Theory (TDDFT)	11
2.3.1	DFT and TDDFT for lattice systems	12
2.3.2	Dynamical Mean Field Theory (DMFT) meets DFT	13
2.4	Non-Equilibrium Green's functions (NEGF)	16
2.4.1	NEGF in steady state	20
2.5	Observables in NEGF and TDDFT	26
2.6	Disorder in nanoscopic systems	27
2.6.1	Binary disorder	28
2.6.2	Box disorder	29
2.7	Disorder using Green's functions	29
2.7.1	Average T-matrix Approximation (ATA)	31
2.7.2	Coherent Potential Approximation (CPA)	32
2.7.3	CPA out of equilibrium	33
2.7.4	Particle conservation for CPA	34
2.7.5	Particle conservation for CPA + 2nd Born	34
3	Numerical methods	37
3.1	Exact Diagonalization	37
3.1.1	Obtaining the ground state	38
3.1.2	Details for the time evolution	39

CONTENTS

3.2	TDDFT	40
3.2.1	Solving the time-independent Kohn-Sham equations	40
3.2.2	Solving the time-dependent Kohn-Sham equations	40
3.3	NEGF	41
3.3.1	Artificial smoothening	43
3.3.2	Details for mixing	44
4	Results	47
5	Conclusions and Outlook	61
	References	65

1

Introduction

The physics of many-body systems, where several particles interact with an external environment as well as with each other, is complex and difficult to describe. Due to their mutual interactions, the motion of one particle is dependent on all the other particles. Such calculations are impossible to do for large systems, and hence one must find another way of tackling the many-body problem. A useful strategy has been to exclude the complicated effects of inter-particle interactions and treat the particles as independent, moving in a mean field which mimics the interactions. This is enough to obtain correct characteristics for many systems, and can, for example, often correctly predict whether a material is a good conductor or not. Moreover, the solution of such independent-particle systems has been a fruitful starting point for perturbative calculations, where the effect of the interaction is treated as a perturbation.

However, there are several cases where the complicated features of interaction effects need to be more carefully considered. Certain materials have shown insulating behavior although independent-electron calculations predict them to be conductors. The opposite is also true - some materials have a much higher conductance than predicted by a non-interacting model. This can be taken as the definition of a strongly correlated system: A system where the interactions can be treated in a satisfactory way neither in a single-particle picture nor by introducing small perturbations. Because of this breakdown, different methods need to be used to correctly describe these systems. A reliable description is important, not only for the vast technological implications that will follow the understanding of nano-scale systems, but also for the fundamentals of many-body physics itself.

1. INTRODUCTION

To be able to focus on the core of the many-body problem, I have been studying model systems rather than real materials. The simplicity permits the models to be solved more easily than their realistic counterparts. Of course, the models must be designed such that they give rise to the same qualitative behavior. At first glance, it could appear that we simplify too much. We model the long-range inter-particle interaction by a short-range interaction. We discretize our system, allowing the particles to exist only on lattice points, 'sites', which have one energy level only. Finally, the particles are allowed to tunnel only to the nearest neighboring lattice sites. However, it turns out that such simple models retain many characteristics of realistic many-body systems. They contain enough physics to capture the essential properties of strongly correlated systems.

Moreover, in recent years, researchers have developed techniques to realize systems with cold atoms in optical lattices. The constraining potentials are created by lasers and can be designed to simulate the periodic potentials from ions in a crystal. The atoms play the role of generic fermions (or bosons), and can be used for modeling electrons. The level of control and flexibility in these systems is unprecedented. Thus, it is possible to construct experimental systems that look very similar to our model systems. In the interplay between such experiments and our model calculations, we can learn not only about the qualitative behavior but also the quantitative features of many-body systems.

The study of many-body systems is one of the most challenging tasks in physics. Tackling such problems can not be done using a single approach, and therefore several methods will be described in this thesis. Many results presented in this thesis will stem from the comparison between such methods, in some cases including exact calculations. It is due to the simplicity of the models we are using, that exact calculations are possible for several cases. This allows us to perform 'numerical experiments' - benchmarks in which different methods and approximations are compared to each other or to exact calculations. This differs from the usual situation in physics, where such benchmarks come from comparing theoretical predictions with experiments. By restricting ourselves to numerical experiments, we can explore the methods without dealing directly with the incompleteness of the model.

The methods used are exact diagonalization, Density Functional Theory (DFT) and its time-dependent extension (TDDFT), and the Non-Equilibrium Green's function

(NEGF) technique. These methods can be utilized not only for model systems but are also routinely used for realistic systems. Exact diagonalization can be used to study few-particle systems in detail. DFT and TDDFT are nowadays two of the most common methods used to describe material properties, while the NEGF technique is starting to gain a foothold in parameter-free calculations.

Each of the methods have their own distinct strengths and weaknesses. Exact diagonalization gives access to the full wavefunction, but can only be used for very small systems. DFT and TDDFT are computationally inexpensive, one of the the major reasons they have gained popularity. However, it is quite difficult to systematically improve the approximations that one must necessarily introduce in practical implementations. NEGF has the advantage that such systematic refinements are possible, but it is an computationally expensive method.

In this thesis, I describe my work with improving upon and developing these methods, and the results thereof. Chapter 2 contains an overview of the theory of the models and methods, and Chapter 3 describes some aspects of the numerics that I have used and developed. Chapter 4 shows selected results from our work, and the last chapter contains my conclusions and outlook.

1. INTRODUCTION

2

Theory

In this chapter, I will introduce the concepts used in the rest of the thesis. I do not make any attempt at being rigorous, but instead I try to give a general picture, and refer to more thorough reviews for further details. I first introduce details about the model studied in this work, and then continue to discuss the main methods for treating the model, namely Density Functional Theory (DFT), Time-Dependent Density Functional Theory (TDDFT) and the Non-Equilibrium Green's Function (NEGF) approach.

2.1 The Model

The models used in this work are several variants of the Hubbard model, introduced by John Hubbard in the mid 60's[1], and is nowadays a well-known model in solid state theory. Being a lattice model, fermions (in case of bosons, the model is called the Bose-Hubbard model) can only exist on lattice sites. Each site has a single energy level, which means that each site can have four different configurations: i) Empty ii) occupied by a single spin-up fermion iii) occupied by a single spin-down fermion iv) doubly occupied by a spin-up and a spin-down fermion. In the case of double occupation, the system gets an energy contribution U , and depending on the sign of U it can act as a repulsion ($U > 0$) or attraction ($U < 0$). Thus, the Coulomb interaction between the fermions is modeled as a contact interaction. The fermions can tunnel from site i to site j , with amplitude J_{ij} . J is also referred to as the hopping term, or more simply, hopping.

2. THEORY

In its simplest form, the Hubbard Hamiltonian is, in second quantization,

$$\hat{H} = \sum_{\langle ij \rangle \sigma} J_{ij} c_{i\sigma}^\dagger c_{j\sigma} + \sum_i U_i c_{i\uparrow}^\dagger c_{i\uparrow} c_{i\downarrow}^\dagger c_{i\downarrow} \quad (2.1)$$

where $\langle ij \rangle$ means that the sum is restricted to nearest neighbors, $\sigma = \uparrow, \downarrow$ denotes spin, c_i^\dagger is a fermionic creation operator which creates a fermion at site i and c_i is the corresponding destruction operator. As stated before, J_{ij} and U_i are the tunneling and interaction terms, respectively. In this form, the Hamiltonian (2.1) can be used for any dimensionality, and for any type of lattice structure. The lattice structure itself is given by the amplitudes J_{ij} . A schematic of the model is shown in Figure 2.1.

The spin-resolved density at each site is given by $\hat{n}_{i\sigma} = c_{i\sigma}^\dagger c_{i\sigma}$, and the total density is thus given by $\hat{n}_i = \hat{n}_{i\uparrow} + \hat{n}_{i\downarrow}$; as such, $n_i = \langle \hat{n}_i \rangle$ can vary between 0 (empty) and 2 (doubly occupied). In all our calculations, we restrict the system to contain an equal number of spin-up and spin-down fermions, and we apply only spin-independent external fields. Thus, at all times $n_i = 2n_{i\uparrow} = 2n_{i\downarrow}$. Because of this, sometimes the term density actually refers to the spin-resolved density.

In this thesis, we use a slightly more general version of the Hamiltonian, in order to study inhomogeneities and time-dependent fields:

$$\begin{aligned} \hat{H}(t) = & \sum_{\langle ij \rangle \sigma} J_{ij} c_{i\sigma}^\dagger c_{j\sigma} + \sum_i U_i \hat{n}_{i\uparrow} \hat{n}_{i\downarrow} + \\ & + \sum_i \epsilon_i \hat{n}_i + \sum_i v_i(t) \hat{n}_i, \end{aligned} \quad (2.2)$$

where we have written the interaction term in terms of the spin-densities instead. ϵ_i are the on-site energies in the system, which can, for example, represent trapping potentials as in Paper I, or randomized disorder as in Papers III and IV. $v_i(t)$ is the time-dependent external field, which is applied to the system to bring it out of equilibrium. $v_i(t)$ can represent, for example, the time-dependent switching-off of the trapping potential, or the applied bias in transport calculations. Note that both the on-site energy and the external fields are local in space.

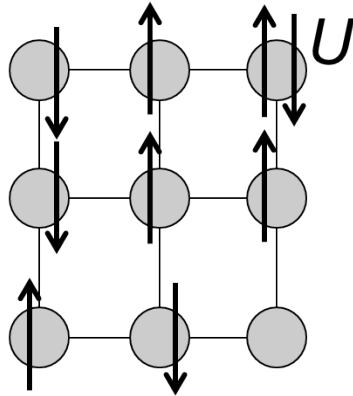


Figure 2.1: A schematic of the lattice model in 2D. When two fermions occupy the same site, they feel an on-site interaction U . The tunneling amplitude from site i to site j is J_{ij} .

The Hubbard model has been applied to many situations in different areas of physics. Books(see e.g. [2]) have been written on the topic of the one-dimensional Hubbard model alone. This is of course because the model, simple as it seems, contains an incredible amount of physics. It was originally developed by Hubbard to describe, as the title of the paper states, *Electron correlations in narrow energy bands*. Since then it has been used to study many other properties, such as magnetism, the Mott metal-insulator transition, high-temperature superconductivity[2], and, more recently, cold atoms in optical lattices, where experiments have confirmed predictions of the Hubbard model, both for bosons and fermions.[3]

I do not attempt to make a deep excursion into the theory behind these models. My perspective is a more practical one; aside from the mathematical properties, there are several reasons for using this model. One is that the model is physically relevant in many situations, like for cold atoms in optical lattices. Another reason is that it is a simple enough so that it can be solved numerically, much more easily than more realistic systems. Thus, in this thesis no numbers are stated in absolute values. We adopt the units $e = \hbar = 1$, and every quantity is given in units of the hopping or inverse hopping. Thus, if the energy is stated as $E = -2$, this means $E = -2J$. Likewise, time is measured in units of inverse hoppings, which means that $t = 2$ is $t = 2\hbar/J$. This arbitrariness is rather versatile; it is possible to use the same type of calculations in electronic systems, and cold atoms systems. In the case of electronic systems, bandwidths are of the order of eVs, giving a hopping that is also of that order. The units of time will then be of the order of femtoseconds. In the case of cold atoms, quantities are often measured in terms of the recoil energy, which sets the energy scale. By using these numbers, the units of time will be of the order of milliseconds.

The Hubbard model in all its forms and dimensionalities are analytically solvable only for a few cases. The exact results useful in my studies are the exact solution for the 1D homogeneous model[4] and the infinite-dimensional homogeneous model[5]. Here, the term homogeneous refers to a system that is infinite in size, and where all parameters are the same for all sites, $U_i = U, J_{ij} = J, \epsilon_i = 0$. I make use of the exact solution in 1D in order to obtain a Local Density Approximation (LDA), usable in inhomogeneous systems in 1D. This is further discussed in the Density Functional Theory (DFT) section2.2. I use the concept of the solution to the infinite-dimensional model as an approximation to 3D, further described in the DMFT section2.3.2.

2. THEORY

For a more thorough review of model Hamiltonians, also combined with DFT, I refer to the recent review by Capelle.[6]

2.2 Density Functional Theory (DFT)

One could argue that the idea behind DFT is reduction. The full knowledge of the wavefunction, obtained by solving the Schrödinger equation, for a moderate number of particles, is not possible, and in fact, not even practical or useful. In experiments, it is the reduced quantities which are of interest, such as energies, densities, or various correlation functions. The wavefunction indeed gives these quantities, but it contains much more information than one is usually interested in. For instance, it is enough to know the one-particle density matrix in order to calculate the kinetic energy of an interacting system. Knowledge of the two-particle density matrix is enough to determine the interaction energy, and thus, the total energy of the system.[7]

In this sense, DFT provides the answer to the question: how far can we push this idea of reduction? The answer from DFT is, that we can reduce the problem to just the density. The density is enough to determine all quantities of the interacting system in the ground state, and in principle also for all excited states.

The reason why this is possible stems from the one-to-one correspondence between the external potential and the particle density, proved by the central theorem in DFT, the Hohenberg-Kohn theorem[8]. The theorem states that the density coming from two different external potentials will always be different. This uniqueness makes it possible to, instead of minimizing the energy with respect to the wavefunction, minimize the energy with respect to the density. This minimization procedure can be done in a very natural way, introduced by Levy[9]. To illustrate the strategy, we first express the ground-state energy as the minimum of the expectation value of the Hamiltonian,

$$E_{gs} = \min_{\psi} \langle \psi | \hat{H} | \psi \rangle = \min_{\psi} \langle \psi | \hat{T} + \hat{U} + \hat{V}_{ext} | \psi \rangle, \quad (2.3)$$

where the external potential is $\hat{V}_{ext} = \sum_i v_i \hat{n}_i$, \hat{T} is the kinetic operator and \hat{U} is the particle-particle interaction.

The strategy used by Levy, now called the Levy restricted search, consists of two consecutive steps to find the ground-state energy. The first step is to pick a density n , and then minimize the energy with respect to all wavefunctions giving this density.

2.2 Density Functional Theory (DFT)

This means that in this subset, the wavefunction is a functional of n , denoted by $\psi[n]$. (A functional $F[n]$ is defined as a rule which takes a function and returns a value. Another example of this is the total number of particles, $N[n] = \int d\mathbf{r}n(\mathbf{r})$, or, in the lattice case, $N[n] = \sum_i n_i$. I call also the latter a function). In this language, the energy is a functional of the wavefunction, $E_{gs} = E_{gs}[\psi]$.

The ground-state energy can thus be written as $E_{gs} = \min_n \min_{\psi \rightarrow n} \langle \psi | \hat{H} | \psi \rangle = \min_n E_v[n]$, where $\psi \rightarrow n$ means the subset of all wavefunctions ψ that yield the density n . The energy $E_v[n]$ is a functional of the density, and since the potential energy does not depend on the explicit shape of the wavefunction, the minimization can be done solely on the interaction and kinetic energy,

$$E_v[n] = \min_{\psi \rightarrow n} \langle \psi | T + U | \psi \rangle + \sum v_i n_i = F[n] + V_{ext}[n] \quad (2.4)$$

where we have defined the (universal) functional $F[n] = \min_{\psi \rightarrow n} \langle \psi | T + U | \psi \rangle$.

The second step is to minimize $E_v[n]$ with respect to the density, which will then yield the ground-state energy, $E_{gs} = \min_n E_v[n] = E_v[n_{gs}]$. In this step, the minimization does not have any explicit dependence on the wavefunction, only on the density, and at the minimum, we have obtained the ground-state energy and density. Also, since we are at the minimum, performing the functional derivative of $E_v[n]$ with respect to the density gives us the external potential, since

$$0 = \frac{\delta F}{\delta n_i} + \frac{\delta V_{ext}}{\delta n_i} = \frac{\delta F}{\delta n_i} + v_i \quad (2.5)$$

The price of hiding the wavefunction shows up in the unknown functional F . This quantity encompasses all the complexities of the many-body problem, and knowledge of F would yield the solution to the original problem. Since obtaining the exact F is as hard as solving the original many-body problem, the remaining question is then how to approximate F in a consistent and useful way. A fruitful is to extract quantities from F which can be obtained more easily, and approximate the rest. The following separation is convenient:

$$F[n] = T_0[n] + T_{xc}[n] + E_H[n] + U_{xc}[n] = T_0[n] + E_H[n] + E_{xc}[n], \quad (2.6)$$

where T_0 is the kinetic energy of a non-interacting system, but with the same density as the original problem, and T_{xc} is the remainder of the kinetic energy. The interaction part is split in a similar way, where the Hartree energy $E_H[n] = \frac{1}{4} \sum_i U_i n_i^2$ has an

2. THEORY

explicit dependence on the density, and the remainder of the interaction energy is U_{xc} . The remainders are then lumped together in the unknown *exchange-correlation* energy E_{xc} . Note that the interacting kinetic energy is defined as, $T[n] = \langle \psi_{min} | \hat{T} | \psi_{min} \rangle$, where $|\psi_{min}\rangle$ is the wavefunction that minimizes $\langle \hat{T} + \hat{U} \rangle$ for a specific density n . On the other hand, $T_0[n] = \min_{\psi \rightarrow n} \langle \hat{T} \rangle$.

Here, we must remark on a specific feature of onsite interactions, such as those studied in our models. For continuous systems, the exchange-correlation energy can be further separated into the exchange energy and the correlation energy. The exchange energy consists of contributions from fermions of the same spin. However, if we write the interaction in a spin-dependent form, as in Eq. 2.1, then there is no exchange, so $E_{xc} = E_c$. Thus, all our quantities should really be denoted E_c instead of E_{xc} , but we write E_{xc} in order to follow common practice in lattice (TD)DFT.

The rewriting into Eq. (2.6) has several advantages. Since the Hartree part is large, as well as the non-interacting kinetic energy, the quantity to be approximated will be smaller. However, it is not obvious how to obtain T_0 as a functional of the density. This problem was solved by Kohn and Sham[10], where they proved that that by constructing a fictitious non-interacting system, designed to reproduce the exact density of the original system, one can obtain T_0 exactly via the non-interacting orbitals of the fictitious system. This is the famous Kohn-Sham system,

$$\left(\hat{T} + \hat{v}_{KS} \right) \varphi_\nu = \epsilon_\nu \varphi_\nu, \quad (2.7)$$

which describes particles that move in an effective local potential. The φ_ν s are the Kohn-Sham orbitals, which make up the wavefunction of the system in a form of a Slater determinant. ϵ_ν are the corresponding Kohn-Sham eigenvalues. The density of the Kohn-Sham system is exactly the same as of the original interacting system, provided that the effective potential v_{KS} is chosen to be

$$v_{KS}(i) = v_{ext}(i) + v_H(i) + v_{xc}[n](i), \quad (2.8)$$

containing the external potential, the Hartree potential $v_H(i) = \frac{1}{2}U_i n_i$, and the exchange-correlation potential $v_{xc}(i) = \frac{\delta E_{xc}}{\delta n_i}$. The density is obtained from the orbitals as

$$n_i = \sum_{\nu}^{occ} |\varphi_\nu(i)|^2. \quad (2.9)$$

2.3 Time-Dependent Density Functional Theory (TDDFT)

Kohn and Sham proved that, if this effective potential exists, it is unique, and will reproduce the density of the interacting system. Under what conditions this potential exists is not a trivial question, and is known as the v_0 representability problem.

The density obtained from the Kohn-Sham system is exact. The only approximation consists of finding a useful expression for the exchange-correlation potential. A quite successful approximation is the Local Density Approximation (LDA), in which the v_{xc} is taken to be the same as for a homogeneous reference system. The approximation assumes that locally, the density behaves as it would in a uniform system. The form of the v_{xc} then becomes $v_{xc}^{LDA}[n] = v_{xc}^{ref}(n)$, which is now an ordinary function. In the majority of DFT calculations, the reference system is taken to be the homogeneous electron gas (Jellium), where the nuclei have been smeared out, only contributing to a positively charged background. In model systems, however, the choice of reference system depends on the specific form of the Hamiltonian. This is discussed in more detail below.

2.3 Time-Dependent Density Functional Theory (TDDFT)

A natural question to ask is if the same philosophy as that of DFT can be applied in the time-dependent domain. Is it possible to, if given the time-dependent density, find the time-dependent potential which gave rise to said density? The answer, for finite systems where the external perturbation tends to zero at infinity, is yes. This was proven by the Runge-Gross theorem[11]. Since this is a time-dependent problem, the initial state has to be specified (not necessarily the ground state). Later, it was also proven by the van Leeuwen theorem[12] that the time-dependent density obtained from a given many-body system, can also be obtained in any other many-body system with a different two-particle interaction. The time-dependent external potential in this new system can be shown to be unique. As a special case, it is possible to find a many-body system with non-interacting particles, which will reproduce the exact density from the interacting system. This is the time-dependent extension to the DFT Kohn-Sham system.

In the time-dependent case, the non-interacting particles move in an effective potential $\hat{v}_{KS}(t)$. As in the ground-state case, we can consider each orbital separately, in

2. THEORY

the Slater determinant which makes up the Kohn-Sham wavefunction. The equations governing this system, for each orbital φ_ν , are

$$\left(\hat{T} + \hat{v}_{KS}(t)\right) \varphi_\nu(t) = i \frac{\partial \varphi_\nu(t)}{\partial t}, \quad (2.10)$$

and the time-dependent density is obtained from the orbitals as

$$n_i(t) = \sum_{\nu}^{occ} |\varphi_\nu(i, t)|^2. \quad (2.11)$$

Similarly to DFT, the time-dependent density of this system is exactly the same as in the original interacting system, provided that the effective potential is chosen to be

$$v_{KS}(i, t) = v_{ext}(i, t) + v_H(i, t) + v_{xc}(i, t), \quad (2.12)$$

where $v_{ext}(t)$ is the time-dependent external potential, $v_H(t) = \frac{1}{2}U_i n_i(t)$ is the Hartree potential, and $v_{xc}(i, t)$ is the time-dependent exchange-correlation potential. The exchange-correlation potential is an extremely complicated object, which depends non-locally on the density, both in space and in time. However, in all our time-dependent calculations, we make use of the Adiabatic Local Density Approximation (ALDA), meaning that $v_{xc}(i, t) \approx v_{xc}^{ALDA}(i, t) = v_{xc}^{LDA}(n_i(t))$, where the LDA is obtained from a homogeneous reference system. This approximation neglects all non-local dependency on the density, both in space time. The problem of how to introduce memory and non-local effects into useful expressions for v_{xc} is still an open problem in TDDFT.

2.3.1 DFT and TDDFT for lattice systems

Whilst ground-state DFT for continuous systems was constructed in the '60s, DFT for lattice systems is a younger concept. It was introduced in the mid '80s by Gunnarson and Schönhammer[13, 14] in order to study the so-called band-gap problem in DFT. Later, the same authors and Noack[15] defined the theory more rigorously, where it was shown that other observables than the density could also be used to construct DFT-like approaches. As a specific case, the lattice density (also called site occupancy) could be used as the basic variable in DFT. Thus, Lattice DFT is sometimes called SOFT (Site Occupancy Functional Theory). Here, an LDA based on the analytically solvable 1D homogeneous Hubbard model[4] was introduced. This is an important difference compared to the interacting electron gas - the paradigm reference system in

2.3 Time-Dependent Density Functional Theory (TDDFT)

ab-initio calculations - where such an analytical solution is not available. The exact LDA introduced had a derivative discontinuity in the exchange-correlation potential at half-filling, which they showed was instrumental in obtaining the correct band gap in their model calculations.

The idea of using different reference systems depending on the system considered was further emphasized by Lima et al[16], in a paper denoted *Density functionals not based on the electron gas: Local-density approximation for a Luttinger liquid*. There, the authors constructed an analytical interpolation of the energy of the 1D Hubbard model as a function of filling. This allows to have an LDA in closed form, making it extremely practical to use in a Kohn-Sham scheme. The LDA from the 1D Hubbard model has been denoted BALDA, which stands for Bethe-Ansatz Local Density Approximation, the name Bethe-Ansatz coming from the technique for solving the 1D homogeneous Hubbard model[4]. BALDA have been favorably benchmarked against exact calculations, showing that this LDA can give results at an accuracy of a few percent for energies, densities and entanglement entropies.[16, 17, 18, 19, 20] Recently, an interpolation valid for the spin-dependent case was constructed[21].

TDDFT for lattices was introduced by Verdozzi[22], where an ALDA was introduced, based on the previously mentioned interpolation scheme in 1D[16]. The question whether it is always possible to find a Kohn-Sham system reproducing the exact density has also been discussed[22, 23]. However, a rigorous proof of the mapping between densities and potentials on a lattice was not done until 2012[24].

For further reading, there are several reviews on the topic of DFT[25] and TDDFT[26, 27] in the continuum formulation, and also for lattices[6, 28].

2.3.2 Dynamical Mean Field Theory (DMFT) meets DFT

Since we made use of DMFT in our TDDFT calculations, I conclude the TDDFT section with a short excursion on DMFT.

In Paper II, we wanted to obtain a LDA usable in 3D systems. This means that we need to be able to solve the homogeneous reference system, the infinite lattice model in 3D. Due to the lack of analytical solutions in 3D, as opposed to 1D where it can be solved by the Bethe-Ansatz, we instead wanted to use a non-perturbative approximation. The reason for this is that in 3D there is a critical transition when the system goes from a metallic behavior to an insulating one, the so-called Mott-Hubbard

2. THEORY

insulator transition, and such phase transitions are hard to capture using perturbative methods.

We used DMFT in order to obtain such an LDA. DMFT is a non-perturbative method usable for both weak and strong interactions. An indirect proof of this is that DMFT is able to describe the metal-insulator transition in the 3D Hubbard model. Thanks to the DMFT reference system, the same type of physics is automatically incorporated into our v_{xc} . Another advantage of the method is that it becomes exact when the number of nearest neighbors tends to infinity, that is, for infinite-dimensional systems.[5]

The idea behind the method is to replace the original lattice problem with an effective model system, containing effective parameters which can be tweaked in order to describe the original system. One of the most popular systems is the Anderson impurity model[29]: A single interacting impurity with the same interaction strength as in the original lattice, is connected via effective parameters to a reservoir, an electron bath. The bath parameters - the single-particle energies and the couplings to the bath - are tuned to mimic the contribution of the original lattice. The local ($R = 0$) Green's function and self-energy from the impurity model are chosen to be equal to the local ones from the lattice,

$$G_{lattice} = G_{impurity} \quad (2.13)$$

$$\Sigma_{lattice} = \Sigma_{impurity}. \quad (2.14)$$

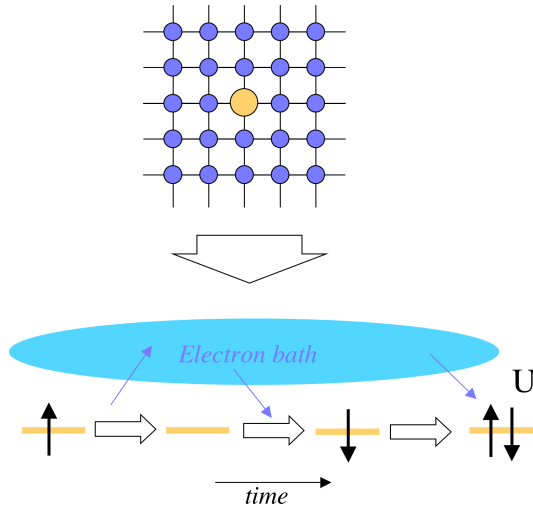


Figure 2.2: A schematic over the Anderson impurity mapping in DMFT. The heat bath can dynamically exchange fermions with the impurity. The parameters of the bath are chosen so that the solutions in the bath is the same as in the original lattice.

2.3 Time-Dependent Density Functional Theory (TDDFT)

The general expression, in (k, ω) -space of the lattice Green's function is

$$G_{lattice}(k, \omega) = \frac{1}{\omega - \epsilon(k) - \Sigma_{lattice}(k, \omega)}. \quad (2.15)$$

The approximation in DMFT (exact in $D = \infty$ dimensions) is that one assumes that the self-energy is k -independent, that is, that the self-energy is local in real space. However, the ω -dependence is kept. The local Green's function is then

$$G_{lattice}(\omega) = \int_{-\infty}^{\infty} \frac{dk^3}{(2\pi)^3} G_{lattice}(k, \omega) e^{ik_0} = \quad (2.16)$$

$$= \int_{-\infty}^{\infty} d\epsilon \frac{\rho_0(\epsilon)}{\omega - \epsilon - \Sigma_{lattice}(\omega)} \quad (2.17)$$

where we have used the single-particle density of states, $\rho_0(\epsilon) = \int \frac{dk^3}{(2\pi)^3} \delta(\epsilon - \epsilon(k))$.

The expression for the local impurity Green's function is

$$G_{impurity}(\omega) = \frac{1}{\omega - \epsilon_0 - \Delta(\omega) - \Sigma_{impurity}(\omega)} \quad (2.18)$$

where Δ is an embedding self-energy, and is determined by the effective parameters of the bath,

$$\Delta(\omega) = \sum_{\nu} \frac{|J_{\nu}|^2}{\omega - \epsilon_{\nu}}, \quad (2.19)$$

where J_{ν} are the hopping parameters from the impurity to the bath, and ϵ_{ν} are the single-particle energies of the bath.

For our calculations, we assumed a finite number of effective parameters, meaning that the impurity and the bath are described as a finite cluster. The finite size permitted us to solve the cluster using exact diagonalization, changing the effective parameters until self-consistency was achieved. In the end of the cycle, quantities like the total energy were extracted. Interestingly, the only input to the DMFT solver is the non-interacting density of states, meaning that the same routine can handle any dimensionality or geometry. However, because of the nature of DMFT, results are expected to be better when increasing the dimensionality[5]. For more details about the method, see [30, 31].

2. THEORY

2.4 Non-Equilibrium Green's functions (NEGF)

Green's function methods have much in common with DFT and TDDFT. Instead of trying to describe the many-body wavefunction with a macroscopic number of coordinates one works with reduced quantities. In the Green's function methods the reduced quantities are few-particle correlation functions, i.e., expectation values or ensemble averages of field operators. A large number of experiments can be expressed directly in terms of such few-particle correlations. For instance, any single-particle quantity such as the density or the current density may be expressed in terms of the one-particle density matrix, optical absorption can be expressed in terms of charge-density correlations, and so on.

The field-theoretical methods originate from particle physics, and since the '50s they have developed into one of the most important theoretical tools in many-body physics. The key quantity is the single-particle Green's function, $G(xt\sigma, x't'\sigma') = \langle \mathcal{T}[\psi_H(xt\sigma)\psi_H^\dagger(x't'\sigma')] \rangle$, where ψ^\dagger, ψ creates (destroys) a particle, and \mathcal{T} is the time-ordering operator. In the original zero-temperature ($T = 0$) technique applicable to ground states, the operators are ordered with respect to real time, which allows for a perturbation expansion to any order via the original Wick theorem. The Wick theorem permits to write time-ordered products in terms of the single-particle Green's function. Later, Matsubara invented a closely related method for ensemble averages with time ordering for imaginary times and a Wick-like theorem for ensemble averages rather than operators. However, neither the original $T = 0$ nor the Matsubara techniques are so well suited for non-equilibrium problems in which a system is brought out of equilibrium by a time-dependent external field. For an overview of the $T = 0$ and Matsubara techniques the reader is referred to Fetter and Walecka[32].

In the path-ordered technique, the previous ordering, real-time or imaginary ordering, is replaced by a time-ordering according to a contour. It contains the earlier techniques as special cases but is directly applicable to non-equilibrium problems and to systems evolving in time-dependent external fields.

The definition of the contour-ordered, single-particle Green's function is, where we use the generalized coordinate $1 = (\mathbf{x}, \sigma, z)$ to encompass space, spin and contour time,

$$G(1, 2) = -iTr \left[\hat{\rho} \mathcal{T}_C(\psi_H(1)\psi_H^\dagger(2)) \right]. \quad (2.20)$$

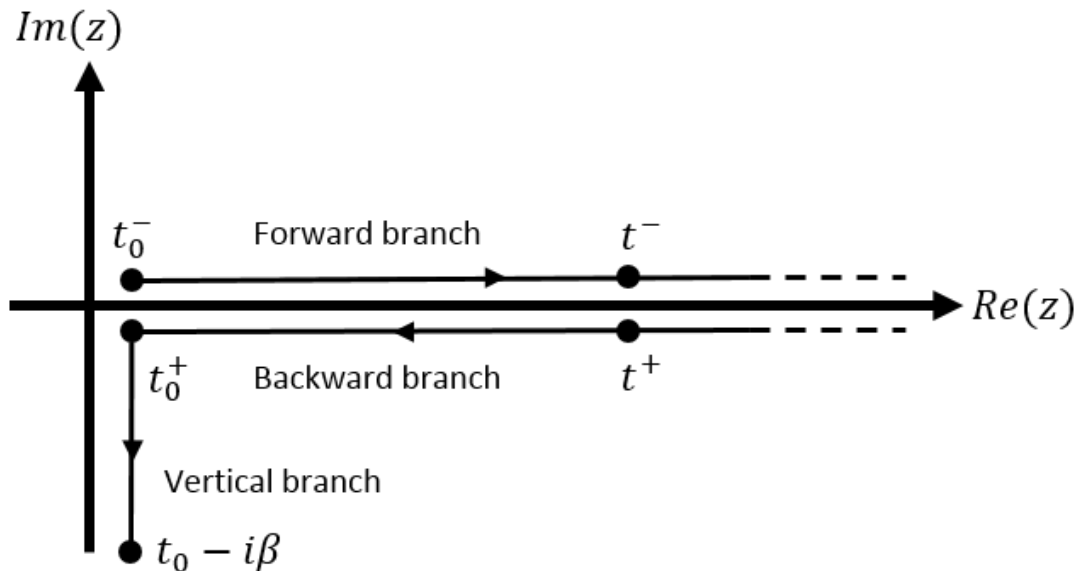


Figure 2.3: Different branches of the contour. The arrows denotes the time ordering of the contour, times on the vertical branch are the latest. All observables are equal on the backward and forward branch, $O(t^+) = O(t^-) = O(t)$. The forward and backward branch are shifted from the real axis only for graphical purposes.

The operator $\hat{\rho} = e^{-\beta\hat{H}^M}/\mathcal{Z}$, with $\hat{H}^M = \hat{H} - \mu\hat{N}$, is the density matrix, which determines the initial state of the system, and the trace is over the Fock space. $\mathcal{Z} = \text{Tr}[e^{-\beta\hat{H}^M}]$ is the partition function, and \mathcal{T}_C is the contour time-ordering operator.

As in the Matsubara formalism, the density matrix can be written as a propagation in imaginary time, $e^{-\beta\hat{H}^M} = e^{-i\int_{\tau_i}^{\tau_f}\hat{H}^M d\tau}$, where $\tau_f - \tau_i = -i\beta$. Additionally, in order to treat systems out of equilibrium, we have to consider time-dependent Hamiltonians, $\hat{H}(t) = \hat{H} + \hat{V}(t)$. Since we now have both real times t and imaginary times τ to deal with, the contour idea comes into play. The contour permits to order operators according to contour times, see Figure 2.3. All operators are extended to have a meaning on the contour. A time variable on the contour is denoted by z , $z = t^-$ on the forward branch, $z = t^+$ on the backward branch, and $z = t_0 - i\tau$ on the imaginary branch. For example, the field operator is defined to be $\psi(x, z) = \psi(x)$, while

$$H(z) = \begin{cases} H + V(t) & \text{if } z = t^-, t^+ \\ H^M = H - \mu N & \text{if } z = -i\tau \end{cases} \quad (2.21)$$

By ordering the quantities according to the contour, one can write Eq. (2.20) as

2. THEORY

$$G(1, 2) = -i \frac{\text{Tr} \left[\mathcal{T}_C(e^{-i \int_\gamma H(z') dz'} \psi(1) \psi^\dagger(2)) \right]}{\text{Tr} \left[e^{-i \int_\gamma H(z') dz'} \right]}. \quad (2.22)$$

This expression can be reduced to the ordinary zero-temperature formalism or the Matsubara formalism, with different choices of the specific form of the contour. For example, the Matsubara formalism follows from the contour only considering the vertical track.

In order to expand the above expression in a perturbation series, we write $H(z) = H_0(z) + H_{int}(z)$, where $H_0(z)$ is a Hamiltonian which is more easily treated, and $H_{int}(z)$ is the remainder. This is a general splitting, but in our case $H_0(z)$ will contain one-body operators, including time-dependent external fields. Under the time-ordering, we can separate the exponential in Eq. (2.22), giving

$$G(1, 2) = -i \frac{\text{Tr} \left[\mathcal{T}_C(e^{-i \int_\gamma H_0(z') dz'} e^{-i \int_\gamma H_{int}(z') dz'} \psi(1) \psi^\dagger(2)) \right]}{\text{Tr} \left[e^{-i \int_\gamma H(z') dz'} \right]} = \quad (2.23)$$

$$= -i \frac{\sum_{k=0}^{\infty} \frac{(-i)^k}{k!} \int \cdots \int_\gamma \langle \mathcal{T}_C(H_{int}(z_1) \cdots H_{int}(z_k) \psi(1) \psi^\dagger(2)) \rangle_0}{\sum_{k=0}^{\infty} \frac{(-i)^k}{k!} \int \cdots \int_\gamma \langle \mathcal{T}_C(H_{int}(z_1) \cdots H_{int}(z_k)) \rangle_0} \quad (2.24)$$

where we have defined $\langle \mathcal{T}_c(\cdots) \rangle_0 = \text{Tr} \mathcal{T}_c(e^{-i \int_\gamma H_0(z') dz'} \cdots)$. If one could find a way to easily calculate contour-time ordered products, one would have a very general and powerful way to obtain the Green's function.

This can be done by a generalization of Wick's theorem[33], reducing the calculations of the perturbation series into terms of non-interacting Green's functions. Then, one can systematically write down the terms and represent them as Feynman diagrams. However, now the Green's functions are functions of contour times, and all integrations have to be performed over the contour. In exactly the same way, higher order Green's functions can be obtained. For a much more thorough treatment on NEGF, see [33]. Expanding in diagrams, one finds the usual Dyson equation, but now generalized for the contour-time-ordered Green's function

$$G(1, 2) = G_0(1, 2) + \int_\gamma d3d4 G_0(1, 3) \Sigma(3, 4) G(4, 2) \quad (2.25)$$

where the self-energy Σ contains all interaction effects. Common approximations to this quantity are Hartree-Fock, 2nd Born, GW and the T-matrix approximation.

2.4 Non-Equilibrium Green's functions (NEGF)

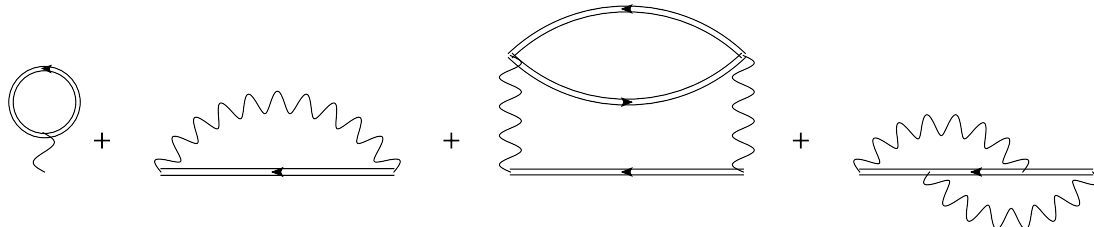


Figure 2.4: All second-order diagrams, which give the 2nd Born approximation. Each Green's function line is the interacting one, which means that $\Sigma = \Sigma[G]$, that is, the diagrams are dressed with the full G . Diagram one and two are referred to as the Hartree-Fock contribution, and the non-local diagrams three and four constitute correlation parts. Note that, if we treat the interactions as spin-dependent, then the second and fourth diagram give zero contribution. If the interactions are treated as spin-independent, then the second diagram, the exchange, will be equal to $-1/2$ of the first diagram, while the fourth diagram will be equal to $-1/2$ of the third diagram. The two ways of treating the interactions are exact, order by order. However, this is no longer true if only a subset of diagrams are summed. In our work, the interactions are always treated as spin-dependent.

A common strategy for dealing with contour integrals is to make use of the so-called Langreth rules, which express the Green's function in real times. Several different components of the Green's function will then exist, depending on the positions of the times on the contour. The components which we will make use of the most are the lesser $G^<$ and greater $G^>$ Green's functions

$$G^>(t, t') = G(t_+, t'_-) \quad (2.26)$$

$$G^<(t, t') = G(t_-, t'_+), \quad (2.27)$$

and the retarded G^R and advanced G^A Green's functions

$$G^R(t, t') = \theta(t - t') (G^>(t, t') - G^<(t, t')) \quad (2.28)$$

$$G^A(t, t') = -\theta(t' - t) (G^>(t, t') - G^<(t, t')). \quad (2.29)$$

The many-body approximation we will make use of consists of all terms up to second order in the interaction, the so-called 2nd Born approximation, see Figure 2.4. The self-energy can be conveniently separated in two parts, $\Sigma_{2B} = \Sigma_{HF} + \Sigma_c$. The Hartree-Fock part is local in time, and this gives $\Sigma_{HF}^{<, >} = 0$. The retarded part is

$$\Sigma_{HF,ij}^R(t, t') = \delta_{ij} \delta(t - t') U_i n_i(t) \quad (2.30)$$

2. THEORY

The correlation part of the 2nd Born self-energy is

$$\Sigma_{c,ij}(t, t') = U_i U_j G_{ij}(t, t') G_{ji}(t', t) G_{ij}(t, t'). \quad (2.31)$$

Note that, differently from Hartree-Fock and Kohn-Sham TDDFT, the quantities are non-local both in time and in space, making such quantities useful for studying memory effects. Note also that the self-energy depend on the interacting Green's function, $\Sigma = \Sigma[G]$. This self-consistent requirement is crucial for conservation laws (particle conservation etc.) to be fulfilled, which is very important in transport setups.

2.4.1 NEGF in steady state

Solving the NEGF is no trivial task. Solving the equations of motion on the contour is computationally very demanding, although it can be done. In this work, we have taken an alternative approach, which is to solve the equations of motion directly in the steady state. This is defined to be the long-time limit (provided it exists) of the equations of motion. All terms related to the initial state are neglected (integrations over the vertical track of the contour), and we are left with simplified equations. In steady-state, all quantities depend on the time difference only, $G(t, t') = G(t - t')$. This permits to conveniently express all equations in frequency space. We work with the retarded $G^R(\omega)$ and lesser $G^<(\omega)$ Green's functions. The Langreth rules give rise to convolutions on the real axis, which have the general form

$$C(t, t') = \int_{t_0}^{\infty} d\bar{t} A(t, \bar{t}) B(\bar{t}, t'). \quad (2.32)$$

In order to treat this in frequency space, we need the Fourier transform in the long-time limit. For long times, the above expression becomes

$$C(t - t') = \int_{t_0}^{\infty} d\bar{t} A(t - \bar{t}) B(\bar{t} - t'). \quad (2.33)$$

Changing variables to $t - \bar{t} = \tau$ (not to be confused with $i\tau$ on the vertical track of the contour)

$$C(t - t') = \int_{-\infty}^{t-t_0} d\tau A(\tau) B(t - \tau - t'), \quad (2.34)$$

we get, in the long time limit $t \rightarrow \infty$, and renaming $t - t' = t$,

$$C(t) = \int_{-\infty}^{\infty} d\tau A(\tau) B(t - \tau). \quad (2.35)$$

2.4 Non-Equilibrium Green's functions (NEGF)

This is a conventional convolution, which means that

$$C(\omega) = A(\omega)B(\omega). \quad (2.36)$$

By using the Langreth rules in time space, it is possible to derive a new set of rules in frequency space. The most useful ones for our purposes are (frequency dependence omitted)

$$c(\omega) = a(\omega)b(\omega) \quad (2.37)$$

$$c^{<,>} = a^R b^{<,>} + a^{<,>} b^R \quad (2.38)$$

$$c^{R,A} = a^{R,A} b^{R,A} \quad (2.39)$$

$$(a^{-1})^{R,A} = (a^{R,A})^{-1} \quad (2.40)$$

$$(a^{-1})^{<,>} = -(a^R)^{-1} a^{<,>} (a^A)^{-1} \quad (2.41)$$

$$(2.42)$$

where the two lower equations can be obtained by applying the Langreth rules to $aa^{-1} = 1$. [34] From these equations, we can derive the following very useful rule (also derived in [35]):

$$c = \frac{a}{1 - ab} = (1 - ab)^{-1} a \quad (2.43)$$

$$c^R = \frac{a^R}{1 - a^R b^R} \quad (2.44)$$

$$c^{<} = \frac{1}{1 - a^R b^R} a^{<} \frac{1}{1 - a^A b^A} + c^R b^{<} c^A \quad (2.45)$$

By going into the long-time limit, the Dyson equation, Eq. (2.25), turns into

$$G(\omega) = G_0(\omega) + G_0(\omega)\Sigma(\omega)G(\omega). \quad (2.46)$$

By making use of the above Langreth rules in frequency space, we obtain the retarded and lesser Green's functions,

$$G^R(\omega) = \frac{1}{\omega - H - \Sigma^R(\omega)} \quad (\text{Dyson equation}) \quad (2.47)$$

$$G^{<}(\omega) = G^R(\omega)\Sigma^{<}(\omega)G^A \quad (\text{Keldysh equation}). \quad (2.48)$$

All calculations are performed in the site basis, which means that all equations above imply matrix multiplications.

2. THEORY

In steady-state, the self-energies has the following form in the long-time limit:

$$\Sigma_{HF,ij}^R(t) = \delta_{ij}\delta(t)U_i n_i \quad (2.49)$$

$$\Sigma_{c,ij}(t) = U_i U_j G_{ij}(t) G_{ji}(-t) G_{ij}(t). \quad (2.50)$$

Following the above rules for converting quantities into frequency space we get, for the retarded part, $\Sigma_{2B}^R = \Sigma_{HF}^R + \Sigma_c^R$, where

$$\Sigma_{HF,ij}^R(\omega) = \delta_{ij} U_i n_i \quad (2.51)$$

$$\Sigma_{c,ij}^R(\omega) = U_i U_j \iint \frac{d\omega' d\omega''}{4\pi^2} \left[\quad (2.52)$$

$$G_{ij}^R(\omega') G_{ji}^<(\omega'') G_{ij}^>(\omega - \omega' + \omega'') + \quad (2.53)$$

$$+ G_{ij}^<(\omega') G_{ji}^A(\omega'') G_{ij}^<(\omega - \omega' + \omega'') + \quad (2.54)$$

$$+ G_{ij}^<(\omega') G_{ji}^<(\omega'') G_{ij}^R(\omega - \omega' + \omega'') \Big], \quad (2.55)$$

while the lesser/greater self-energy is $\Sigma_{2B}^{<, >} = \Sigma_c^{<, >}$, where

$$\Sigma_{c,ij}^{<, >}(\omega) = U_i U_j \iint \frac{d\omega' d\omega''}{4\pi^2} G_{ij}^{<, >}(\omega') G_{ji}^{>, <}(\omega'') G_{ij}^{<, >}(\omega - \omega' + \omega''). \quad (2.56)$$

The relations

$$(G^R)^\dagger(\omega) = G^A(\omega) \quad (2.57)$$

$$(G^{<, >})^\dagger(\omega) = -G^{<, >}(\omega) \quad (2.58)$$

$$G^> - G^< = G^R - G^A = -2\pi i A \quad (2.59)$$

can be used to write the self-energies as functions of G^R and $G^<$ only. A is the non-equilibrium spectral function.

In principle, we have now all ingredients we need. To obtain the Green's function for any system, we solve the Dyson equation with the chosen many-body approximation. However, since we are interested in transport calculations, we would have to consider the Green's function in the central region and in the leads, at the same time. However, it has been shown[36, 37], that if we have a central region connected to macroscopic non-interacting reservoirs, such as leads, it is possible to find an effective equation for the central region, where the effect of lead α can be accounted for by introducing an additional self-energy, Σ_α , the so-called embedding self-energy from lead α . The sum

2.4 Non-Equilibrium Green's functions (NEGF)

of all reservoirs give the total embedding self-energy, $\Sigma_{emb} = \sum_{\alpha} \Sigma_{\alpha}$. The shape of the embedding self-energy depends only on the unconnected reservoirs, and can thus be calculated beforehand. This means that the Dyson equation, Eq. (2.25), can be written in terms of the contacted system alone, and then reads

$$G(1, 2) = G_0(1, 2) + \int_{\gamma} d3d4 G_0(1, 3) (\Sigma_{MB}(3, 4) + \Sigma_{emb}(3, 4)) G(4, 2). \quad (2.60)$$

where now all Green's functions and self-energies are in the central region only. G_0 is the Green's function for the uncontacted central region, and the total self-energy is the sum of the many-body self-energy and the embedding self-energy, $\Sigma = \Sigma_{MB} + \Sigma_{emb}$. The same technique was used when discussing the Anderson model, see section 2.3.2. For our purposes, we consider one-dimensional semi-infinite leads, which permits an analytic expression of the embedding self-energy. It is non-zero only where the leads connect to the central region and can be expressed as $(\Sigma_{\alpha}^R(\omega))_{ij} = \delta_{ij} \delta_{i\alpha} \sigma^R(\omega - b_{\alpha})$, where $\delta_{i\alpha}$ specifies the site in the central region where lead α is connected, and b_{α} is the bias applied to lead α . The exact form for the embedding self-energy in 1D is[33], in units of the hopping parameter $J = 1$,

$$\sigma^R(x) = \frac{1}{2} \begin{cases} x - \sqrt{x^2 - 4} & \text{if } x > 2 \\ x - i\sqrt{4 - x^2} & \text{if } |x| \leq 2 \\ x + \sqrt{x^2 - 4} & \text{if } x < -2. \end{cases} \quad (2.61)$$

This lead has a finite bandwidth and sharp edges. This is difficult to handle numerically when performing operations such as convolutions, and thus we make use of a smoothed lead. The explicit shape of the self-energy is taken to be

$$\sigma^R(z_{\alpha}) = \frac{2}{z_{\alpha} + \text{sgn}(\text{Re}(z_{\alpha})) \sqrt{z_{\alpha}^2 - 4}}, \quad (2.62)$$

where $z_{\alpha} = \omega - b_{\alpha} + i\eta$ and η is the smoothing of the lead, see Figure 2.5.

The lesser/greater embedding self-energy has the same matrix structure as the retarded self-energy, $(\Sigma_{\alpha}^{<,>}(\omega))_{ij} = \delta_{ij} \delta_{i\alpha} \sigma_{\alpha}^{<,>}(\omega)$, where[38]

$$\sigma_{\alpha}^{<}(\omega) = i f(\omega - \mu_{\alpha} - b_{\alpha}) \Gamma(\omega - b_{\alpha}) \quad (2.63)$$

$$\sigma_{\alpha}^{>}(\omega) = i [f(\omega - \mu_{\alpha} - b_{\alpha}) - 1] \Gamma(\omega - b_{\alpha}). \quad (2.64)$$

The symbol f denotes the Fermi-Dirac distribution, μ_{α} is the chemical potential of lead α and $\Gamma(\omega) = -2\text{Im} [\sigma^R(\omega)]$ is the effective coupling to the lead. We also consider

2. THEORY

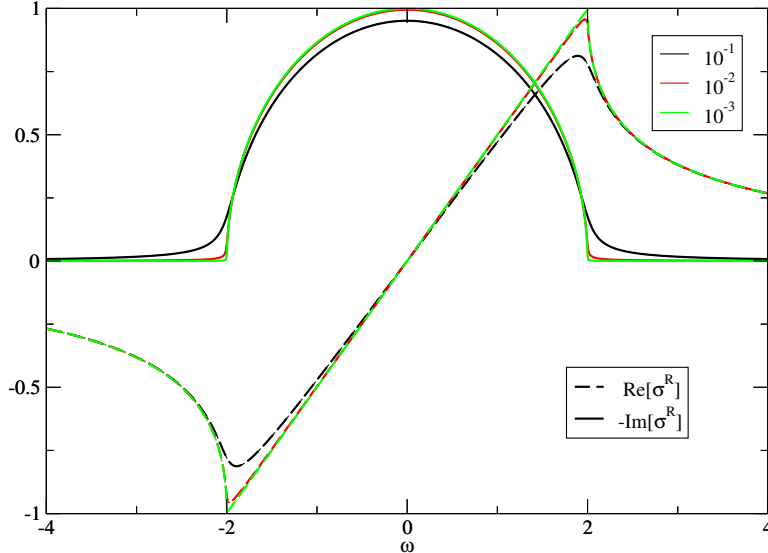


Figure 2.5: The embedded self-energy σ^R for different values of the lead smoothening parameter η . In the simulations, $\eta = 10^{-2}$ was often used. However, a more smooth self-energy was needed to converge CPA calculations.

leads which are featureless, that is, independent on frequency. This so-called wide-band limit is defined as $\sigma^R(\omega) = -i\eta$. This will give a frequency-independent coupling, $\Gamma(\omega) = 2\eta$.

At self-consistency, we calculate several quantities of interest, such as the density

$$n_i = \int \frac{d\omega}{2\pi i} G_{ii}^<(\omega), \quad (2.65)$$

and the current I_α from lead α , obtainable from the Meir-Wingreen formula[39],

$$I_\alpha = \int_{-\infty}^{\infty} \frac{d\omega}{2\pi i} Tr [\Gamma^\alpha (G^< - 2\pi i f_\alpha A)], \quad (2.66)$$

where the trace is taken over the central region.

The Meir-Wingreen formula, Eq. (2.66) is a generalization of the Landauer-Büttiker formula, which states that for non-interacting systems, the current is given by the difference of the Fermi distributions in the leads, times the transmission function,

$$I = \int \frac{d\omega}{2\pi} (f_L - f_R) T(\omega), \quad (2.67)$$

where $T(\omega) = Tr[\Gamma^L G^R \Gamma^R G^A]$. The Meir-Wingreen formula reduces to the Landauer-Büttiker formula for non-interacting systems. In the case of an interacting system, we

2.4 Non-Equilibrium Green's functions (NEGF)

can separate the self-energy into $\Sigma = \Sigma_{emb} + \Sigma_{MB}$ and define generalized 'transmission functions' $U(\omega)$ and $V(\omega)$;

$$U_{\alpha c} = Tr[\Gamma^\alpha G^R i\Sigma_c^< G^A] \quad (2.68)$$

$$V_{\alpha c} = Tr[\Gamma^\alpha G^R (i\Sigma_c^> - i\Sigma_c^<) G^A], \quad (2.69)$$

where $i\Sigma^<$ is a hermitian matrix, resulting in real-valued transmission functions. With these definitions, the current formula for an interacting system can be written as

$$I = \int_{-\infty}^{\infty} \frac{d\omega}{2\pi} [(f_L - f_R)T(\omega) + U_{Lc}(\omega) + f_L V_{Lc}(\omega)]. \quad (2.70)$$

This is merely a rewriting of the Meir-Wingreen formula, and thus gives the exact current if the exact self-energy is used. In this form, however, it is clear that the concept of a Landauer-like transmission function is less defined for the interacting case. It should be noted that even if U and V would be neglected, Eq. (2.70) still contains effects of the interaction via G^R . This means that the resulting transmission function will differ from the non-interacting one.

Another quantity which we calculate is the double occupancy, a sensitive measure for assessing approximations, but also an ingredient in entanglement measures. We calculate the double occupancy as in [40], but for numerical convenience we split the self-energy into a Hartree-Fock part and a correlation part. Doing this, we obtain

$$\langle n_{k\uparrow} n_{k\downarrow} \rangle(t) = n_k^2(t) - \frac{i}{U_k} \int_{\gamma} (\Sigma_c(tz) G(zt^+))_{kk} dz. \quad (2.71)$$

In the case of mean-field where $\Sigma_c = 0$, we automatically end up with the correct non-interacting double occupancy. In the limit of small interactions the correlation self-energy tends to zero as U^2 when $U \rightarrow 0$, and thus Eq. (2.71) is still well-defined. A limiting procedure has to be taken, however, if one studies a interacting cluster where the fermions are non-interacting on one or more sites. In the long-time limit, we end up with the following expression in frequency space

$$d_k = \langle n_{k\uparrow} n_{k\downarrow} \rangle = n_k^2 + \frac{1}{U_k} \int_{-\infty}^{\infty} \frac{d\omega}{2\pi i} (\Sigma_c^<(\omega) G^A(\omega) + \Sigma_c^R(\omega) G^<(\omega))_{kk}. \quad (2.72)$$

Knowing the density and the double occupancy, the single-site entanglement entropy \mathcal{E}_k in equilibrium is defined as[41, 42]

$$\mathcal{E}_k = -2(n_k - d_k) \log_2(n_k - d_k) - d_k \log_2(d_k) - (1 - 2n_k + d_k) \log_2(1 - 2n_k + d_k). \quad (2.73)$$

We use this formula generalized to out-of-equilibrium situations.

2. THEORY

2.5 Observables in NEGF and TDDFT

The strategy for obtaining useful quantities in NEGF and TDDFT are quite different. In NEGF, knowledge of the single-particle Green's function will yield all time-dependent single-particle quantities, such as currents and particle densities. In general, the two-particle Green's function is needed to calculate two-particle quantities, but in certain cases one can still find expressions in terms of the single-particle Green's function. One example mentioned before is the double occupancy, another is the total energy of a system.

The strategy in TDDFT is different. The theory promises that all quantities are obtainable from the time-dependent density, but finding useful expressions for observables is far from trivial. The introduction of the Kohn-Sham system provides an efficient way of obtaining the density, as well as the non-interacting kinetic energy. Moreover, the highest occupied Kohn-Sham eigenvalue yields the ionization energy[43]. One has to be careful in attributing other Kohn-Sham properties any actual meaning. For example, the Kohn-Sham current does not have to be the same as the real current. However, via the continuity equation

$$\frac{\partial n}{\partial t} = -\nabla \cdot J \quad (2.74)$$

one can state that the Kohn-Sham longitudinal current - the one that changes the density - must be equal to the true longitudinal current. The transverse current, however, is not directly obtainable in TDDFT.

Of course, if one can find an explicit expression of a quantity in terms of the density, then we are guaranteed that this is an exact relation. Examples include the potential energy and the Hartree energy, but also more non-trivial ones like the conductance in single-channel junctions. [44, 45]

In order to obtain other quantities in TDDFT, one can resort to different tricks. One is to assume an ALDA strategy, which is to say that the quantity in the homogeneous reference system is approximately the same as in the inhomogeneous system. An example of this is the double occupancy $\langle n_{i\uparrow}n_{i\downarrow} \rangle$. Since the energy per site in the homogeneous system is $e = T/L + U\langle n_{\uparrow}n_{\downarrow} \rangle$, the double occupancy can be obtained as

$$\frac{\partial e}{\partial U} = \langle n_{\uparrow}n_{\downarrow} \rangle. \quad (2.75)$$

Since $e = e(n)$, the double occupancy is also a function of n . Using an interpolation for the energy[16] gives an explicit expression for the double occupancy. This can then be used as an LDA for inhomogeneous systems in the ground state[20] or as an ALDA in the time-dependent case. The latter was introduced by us[46];

$$\langle n_{i\uparrow}n_{i\downarrow} \rangle(t) = \frac{\partial e(n_i(t))}{\partial U}. \quad (2.76)$$

As a side remark, the Kohn-Sham double occupancy is simply the non-interacting quantity $\langle n_{i\uparrow} \rangle \langle n_{i\downarrow} \rangle = n_i^2/4$.

2.6 Disorder in nanoscopic systems

Since a considerable part of this thesis deals with disordered systems, I would here like to discuss fundamental aspects of such systems. I will only discuss so-called diagonal disorder, meaning that the disorder perturbation is local, and can be written as

$$H = \hat{T} + \sum_n |n\rangle V_n \langle n| = \hat{H}_0 + \hat{V}, \quad (2.77)$$

where V_n is the diagonal disorder. In each disorder configuration, the numbers V_n will be different, and their behavior will be determined by their probability distributions. This is defined in the following way: for L sites, we have the total probability distribution function

$$P(V_1, V_2 \dots V_L) \equiv P(\{V_n\}). \quad (2.78)$$

The probability distribution is normalized, meaning that

$$\int \dots \int \{dV_n\} P(\{V_n\}) = 1. \quad (2.79)$$

The average value with respect to disorder is taken to be

$$\langle G \rangle = \int \dots \int \{dV_n\} P(\{V_n\}) G(\{V_n\}). \quad (2.80)$$

In this work, we are interested in the case of uncorrelated disorder. This means that V_i cannot affect V_j , and thus the probability distribution factorizes. The probability distribution in this case becomes

$$P(\{V_n\}) = \prod_n p(V_n) = p(V_1)p(V_2) \dots p(V_n). \quad (2.81)$$

2. THEORY

The separate probability functions are assumed to be separately normalized. This means that for the average value becomes

$$\langle G \rangle = \int \cdots \int \{dV_n\} \prod_n (p(V_n)G(\{V_n\})), \quad (2.82)$$

and generally no further simplification can be done.

However, if we consider a quantity $t_m(V_m)$ which depends only on V_m ,

$$\langle t_m \rangle = \int \cdots \int \{dV_n\} \prod_n p(V_n) t_m(V_m) = \int dV_m p(V_m) t_m(V_m), \quad (2.83)$$

or, equivalently,

$$\langle t_m \rangle = \int dV p(V) t_m(V). \quad (2.84)$$

Thus, quantities at different sites factorize:

$$\langle t_m t_n \rangle = \int dV p(V) t_m(V) \int dV p(V) t_n(V) = \langle t_m \rangle \langle t_n \rangle, \quad (2.85)$$

but, if they are at the same site,

$$\langle t_n t_n \rangle = \int dV p(V) t_n^2(V) = \langle t_n^2 \rangle \neq \langle t_n \rangle^2. \quad (2.86)$$

We consider two types of probability distributions in this work, binary disorder and box disorder. There are of course many more, including speckle disorder, used in optical lattices. For simplicity, we exclude correlated disorder from our studies.

2.6.1 Binary disorder

Binary disorder is often used to model alloys and doped semiconductors. In binary disorder, there are two types of atoms. Atoms of type A have an on-site energy V_A , and concentration c . Atoms of type B have an on-site energy V_B , and concentration $1 - c$. The explicit probability distribution is

$$p(V) = c\delta(V - V_A) + (1 - c)\delta(V - V_B), \quad (2.87)$$

and an average will yield

$$\langle t_m \rangle = ct_m(V_A) + (1 - c)t_m(V_B). \quad (2.88)$$

For fixed concentration of $c = N_A/L$ and for finite systems, complete averaging can be done. The total number of different disorder configurations is $\binom{L}{N_A}$.

2.6.2 Box disorder

Box disorder of strength W means that for every site, the energy is drawn from a random number from the interval $[-W/2, W/2]$. The probability function is then

$$p(V) = \begin{cases} 1/W & \text{if } |V| < W/2 \\ 0 & \text{otherwise.} \end{cases} \quad (2.89)$$

Differently from the binary disorder, for box disorder there is no possibility of performing a full numerical average. Instead only partial averaging can be done, and one has to check that quantities are converged with respect to the number of disorder configurations.

2.7 Disorder using Green's functions

For each disorder configuration, the Dyson equation, as well as the equation for the T-matrix (the formula below can be seen as a definition of the T-matrix), will be

$$G = G_0 + G_0 \hat{V} G \quad (2.90)$$

$$G = G_0 + G_0 \hat{T} G_0, \quad (2.91)$$

where \hat{V} and \hat{T} will depend on the specific disorder configuration. Disorder averaging will give

$$\langle G \rangle = G_0 + G_0 \langle \hat{V} G \rangle \quad (2.92)$$

$$\langle G \rangle = G_0 + G_0 \langle \hat{T} \rangle G_0. \quad (2.93)$$

In general, one cannot easily describe $\langle VG \rangle$. The exact way of obtaining the average would be to do a large set of calculations using different random numbers, and then take the average. This is one of the approaches followed in this work.

However, such numerical disorder averaging is computationally expensive, and thus, approximate methods of obtaining disorder averages has been constructed. One very useful strategy is to find an effective medium, that is, an auxiliary system with effective parameters, tailored to describe the arithmetical average of the original system. This is very similar to the DMFT idea (described in section 2.3.2) where the effective medium was the heat bath. One advantage with the Green's function approach is that the

2. THEORY

properties of the effective medium is quite naturally expressed by its self-energy, just as in the case of DMFT.

One approximation for averages, which was one of the first to be used[47], is the Virtual Crystal Approximation (VCA). This corresponds to making the approximation $\langle VG \rangle \approx \langle V \rangle \langle G \rangle$. VCA simply shifts the energies of the non-disordered system with the average disorder energy, since $G = (G_0^{-1} - \langle V \rangle)^{-1}$. This approximation misses many features of disordered systems, but it shows the idea of introducing an effective medium in order to deal with disorder.

The properties of the effective medium can be obtained quite naturally in a Green's function framework. Consider the average of Eq. (2.90), which will then define the self-energy Σ for the effective medium,

$$\langle G \rangle = G_0 + G_0 \langle \hat{V} G \rangle := G_0 + G_0 \Sigma \langle G \rangle, \quad (2.94)$$

Equation (2.94) is an exact equation, and thus knowledge of the self-energy Σ will yield the averaged Green's function. The equation can be rewritten as

$$\langle G \rangle = \frac{1}{G_0^{-1} - \Sigma} \quad (2.95)$$

where, in contrast to VCA, Σ is not simply the average of V , but is instead non-local, complex and energy-dependent. Of course, finding the true Σ is as hard as solving the original problem.

Let us turn to the problem of approximating this quantity. Since the effective medium is designed to take disorder into account, one could gain insight from treating $\hat{V} - \hat{\Sigma}$ as a perturbation. Eqs. (2.90, 2.91) become

$$G = \langle G \rangle + \langle G \rangle (\hat{V} - \hat{\Sigma}) G \quad (2.96)$$

$$G = \langle G \rangle + \langle G \rangle \hat{T}' \langle G \rangle. \quad (2.97)$$

Taking the average of Equation (2.97), we find the exact condition for the T-matrix from the medium: $\langle T' \rangle = 0$. This means that there will be, on average, no additional scattering from the effective medium. From Eq. (2.96) and Eq. (2.97) it is straightforward to find a matrix equation relating the T-matrix to the self-energy:

$$T' = (1 - (V - \Sigma) \langle G \rangle)^{-1} (V - \Sigma). \quad (2.98)$$

In the case of only one impurity of energy V_m at site m in an otherwise homogeneous system, the scattering matrix has the simple form $T_m = |m\rangle t_m \langle m|$, where t_m is the local t-matrix at site m ,

$$t_m = \frac{V_m}{1 - V_m G_0(m, m)}. \quad (2.99)$$

In the case of several impurities, the T-matrix is not equal to the sum of local T-matrices due to interference effects between the scatterers. Instead, one can show that the explicit form of T' is (Economou, Equation (7.69)[48]),

$$T' = \sum_m T_m + \sum_{n \neq m} T_n \langle G \rangle T_m + \sum_{n \neq m \neq l} T_n \langle G \rangle T_m \langle G \rangle T_l + \sum_{n \neq m \neq l \neq k} T_n \langle G \rangle T_m \langle G \rangle T_l \langle G \rangle T_k + \dots \quad (2.100)$$

Thus, to first order, the scattering matrix is the sum of the individual t -matrices, and the higher order terms contain multiple scattering events.

2.7.1 Average T-matrix Approximation (ATA)

To find an equation for the effective medium, we have to resort to approximations. In the ATA, one assumes that the self-energy is local in space, $\Sigma_{ij} = \delta_{ij} \Sigma_i$. Thus, Σ can be seen as a local potential (albeit complex and energy-dependent). Note that Σ_i is site-dependent, which differs from the usual treatments where the non-disordered system is homogeneous.

The total scattering matrix T in the original system will be a very complicated function of all t_m s for all sites m of the system. The local scattering matrix for the effective medium is, similarly,

$$t'_m = \frac{\Sigma_m}{1 - \Sigma_m G_0(m, m)} \quad (2.101)$$

where Σ_m does not depend on a specific disorder configuration. The ATA consists of making the approximation $\langle t_m \rangle = t'_m$. This is enough to determine Σ_m :

$$\langle t_m \rangle = \frac{\Sigma_m}{1 - \Sigma_m G_0(m, m)}. \quad (2.102)$$

As an example, in the case of binary disorder, this means that

$$\langle t_m \rangle = c \frac{V_A}{1 - V_A G_0(m, m)} + (1 - c) \frac{V_B}{1 - V_B G_0(m, m)}. \quad (2.103)$$

2. THEORY

Thus, from the condition (2.102), the self-energy is completely determined. It is complex, since G_0 is complex. When we have determined Σ , we obtain the averaged G from

$$\langle G \rangle = \frac{1}{\omega - H_0 - \Sigma(\omega)}. \quad (2.104)$$

In the ATA, the effect of the disorder is more than a rigid shift as in the VCA; the spectrum will be broadened because of the finite imaginary part, and the energy shift will not be rigid since the self-energy is frequency dependent.

2.7.2 Coherent Potential Approximation (CPA)

The CPA also assumes a local self-energy, as in ATA, called the coherent potential. As opposed to the ATA, however, the CPA does not assume that the averaged local t -matrices are equal to the ones of the effective medium. Instead, CPA is constructed to fulfill the exact condition for the T -matrix in some limit, $\langle T' \rangle = 0$. The form of the T -matrix is given in Equation (2.98), but it is not easily solved, even for the case of a local self-energy. Instead, it is assumed that the local t -matrix of the effective medium is equal to zero, giving

$$\langle t_m \rangle = \left\langle \frac{V_m - \Sigma_m}{1 - (V_m - \Sigma_m)\langle G_m \rangle} \right\rangle = 0. \quad (2.105)$$

The frequency dependence is omitted, and we write $\langle G(m, m) \rangle = \langle G_m \rangle$ for notational simplicity. Eq. (2.105) is referred to as the CPA condition[49]. While similar in structure to the ATA, the self-energy now has to be determined self-consistently. A computational advantage is that all quantities are local in space, meaning that we can solve the self-consistent loop for each site.

The approximation in CPA will give $\langle t_m \rangle = 0$, for all sites m . However, this does not mean that the exact condition $\langle T' \rangle = 0$ is fulfilled. Examining the terms in Eq. (2.100), this means that the three first terms are zero, since for uncorrelated disorder, $\langle t_1 t_2 \rangle = \langle t_1 \rangle \langle t_2 \rangle$. The fourth term, however, contains terms like $\langle t_1 t_2 t_1 t_2 \rangle = \langle t_1^2 \rangle \langle t_2^2 \rangle \neq 0$. Thus, CPA treats certain multiple scatterings from the same sites incorrectly.

Since we have used CPA for binary disorder, the specific form of the CPA condition, Eq. (2.105), is

$$c \frac{V_A - \Sigma_m}{1 - (V_A - \Sigma_m)\langle G_m \rangle} + (1 - c) \frac{V_B - \Sigma_m}{1 - (V_B - \Sigma_m)\langle G_m \rangle} = 0. \quad (2.106)$$

2.7.3 CPA out of equilibrium

To use CPA out of equilibrium in transport calculations, that is, in presence of a bias, the CPA condition Eq. 2.105 has to be generalized. This can be done using so-called vertex corrections, done in linear response[50], and out of equilibrium[51]. However, from a NEGF perspective, it is quite natural to view the non-equilibrium properties as coming from quantities which are contour ordered. This was done in[34], where they showed that this approach yielded the non-equilibrium vertex corrections.

We thus consider the contour-ordered CPA condition

$$\langle t_m \rangle = \left\langle \frac{V_m - \Sigma_m}{1 - (V_m - \Sigma_m)\langle G_m \rangle} \right\rangle = 0. \quad (2.107)$$

Making use of the Langreth rules, Eq. (2.39,2.40), the retarded part of Eq. (2.107) gives us back the original CPA condition

$$\langle t_m^R \rangle = \left\langle \frac{V_m - \Sigma_m^R}{1 - (V_m - \Sigma_m^R)\langle G_m^R \rangle} \right\rangle = 0, \quad (2.108)$$

which means that in equilibrium, where we need only the retarded part, the formalism is identical. However, out of equilibrium, we need an additional quantity, for example $G^<$. This yields a lesser self-energy $\Sigma^<$, which needs to be treated as well.[34]

By applying a Langreth rule, Eq. (2.45), to Eq. (2.107), we obtain

$$0 = \langle t_m^< \rangle = - \left\langle \frac{1}{1 - (V_m - \Sigma_m^R)\langle G_m^R \rangle} \Sigma_m^< \frac{1}{1 - (V_m - \Sigma_m^A)\langle G_m^A \rangle} \right\rangle + \langle t^R \langle G_m^< \rangle t^A \rangle. \quad (2.109)$$

Now, since the self-energy is independent on disorder averaging, and all quantities are local, we can solve this equation for the lesser self-energy:

$$\Sigma_m^< = \langle G_m^< \rangle \frac{\left\langle \left| \frac{V_m - \Sigma_m^R}{1 - (V_m - \Sigma_m^R)\langle G_m^R \rangle} \right|^2 \right\rangle}{\left\langle \left| \frac{1}{1 - (V_m - \Sigma_m^R)\langle G_m^R \rangle} \right|^2 \right\rangle} = \langle G_m^< \rangle \frac{\langle |t_m^R|^2 \rangle}{\left\langle \left| \frac{1}{1 - (V_m - \Sigma_m^R)\langle G_m^R \rangle} \right|^2 \right\rangle} = \langle G_m^< \rangle f_m, \quad (2.110)$$

valid for any type of uncorrelated disorder distribution. Here, $f_m = f(\langle G_m^R \rangle, \Sigma_m^R)$ is a real, non-negative function. We summarize the two CPA conditions in frequency space:

$$0 = \left\langle \frac{V_m - \Sigma_m^R(\omega)}{1 - (V_m - \Sigma_m^R(\omega))\langle G_m^R(\omega) \rangle} \right\rangle \quad (2.111)$$

$$\Sigma_m^<(\omega) = \langle G_m^<(\omega) \rangle f(\langle G_m^R \rangle, \Sigma_m). \quad (2.112)$$

2. THEORY

Equations (2.111, 2.112) define CPA out of equilibrium. The equations are local, both in space and in frequency. Moreover, since Σ^R does not depend on the lesser components, an existing ground-state CPA solver can be used, in conjunction with the equation for the lesser component. Finally, the explicit form of the lesser CPA self-energy can be used to prove particle conservation in a rather elegant way, see below.

2.7.4 Particle conservation for CPA

In this section, we show that the single-site CPA conserves the particle number in a transport setup. It can be shown from the Meir-Wingreen formula, Eq. (2.66) that the difference in the currents from the leads, ΔI , can be written as [52]

$$\Delta I = \int_{-\infty}^{\infty} \frac{d\omega}{2\pi} \text{Tr} [\Sigma_c^< G^> - \Sigma_c^> G^<], \quad (2.113)$$

where $\Sigma_c = \Sigma - \Sigma_{emb}$ contains the self-energy parts beyond the embedding self-energies. In the present case, we do not consider interactions beyond mean field, and thus $\Sigma_c^{<, >} = \Sigma_{CPA}^{<, >}$. Any conserving approximation will have $\Delta I = 0$. Particle conservation follows from the explicit form of the lesser/greater CPA self-energy, Eq. (2.112). The integrand in Eq. (2.113) can then be expressed as

$$\sum_i (\Sigma_{CPA}^<)_{ii} G_{ii}^> - (\Sigma_{CPA}^>)_{ii} G_{ii}^< = \quad (2.114)$$

$$= \sum_i G_{ii}^< f_i G_{ii}^> - G_{ii}^> f_i G_{ii}^< = 0. \quad (2.115)$$

This holds for any number of sites, and also for any number of leads. It holds for any interaction which has a self-energy local in time such as Hartree-Fock or Kohn-Sham density functional theory, and also any type of uncorrelated disorder.

2.7.5 Particle conservation for CPA + 2nd Born

The simplest way of treating interactions beyond the mean-field level, is to treat the 2nd Born self-energy and the CPA self-energy as additive. It is not obvious that the result will be conserving, see Paper V[53]. Here, we prove particle conservation explicitly. We again make use of Eq. (2.113), where the previous arguments still hold for the CPA part. Thus, we only need to consider on the 2nd Born part.

In 2nd Born, the self-energy is local in time, see Eq. (2.31). Thus it is more convenient to consider Eq. (2.113) in frequency space,

$$\Delta I = \int_{-\infty}^{\infty} dt \text{Tr} [\Sigma^{<}(t)G^{>}(-t) - \Sigma^{>}(t)G^{<}(-t)] = \quad (2.116)$$

$$= \sum_{kl} \int_{-\infty}^{\infty} dt [\Sigma_{kl}^{<}(t)G_{lk}^{>}(-t) - \Sigma_{kl}^{>}(t)G_{lk}^{<}(-t)] = \quad (2.117)$$

$$= \sum_{kl} U_k U_l \int_{-\infty}^{\infty} dt \left[G_{kl}^{<}(t)G_{lk}^{>}(-t)G_{kl}^{<}(t)G_{lk}^{>}(-t) - \right. \quad (2.118)$$

$$\left. - G_{kl}^{>}(t)G_{lk}^{<}(-t)G_{kl}^{>}(t)G_{lk}^{<}(-t) \right]. \quad (2.119)$$

Using the fact that $G_{kl}^{<,>}(-t) = -[G_{lk}^{<,>}(t)]^*$, we get (all quantities are now at the same t , so we omit time-dependence),

$$\Delta I = \sum_{kl} U_k U_l \int_{-\infty}^{\infty} dt G_{kl}^{<}(G_{kl}^{>})^* G_{kl}^{<}(G_{kl}^{>})^* - \quad (2.120)$$

$$- G_{kl}^{>}(G_{kl}^{<})^* G_{kl}^{>}(G_{kl}^{<})^* = \quad (2.121)$$

$$= \sum_{kl} U_k U_l \int_{-\infty}^{\infty} dt \left[[G_{kl}^{<}]^2 [(G_{kl}^{>})^*]^2 - [G_{kl}^{>}]^2 [(G_{kl}^{<})^*]^2 \right] = \quad (2.122)$$

$$= 2i \sum_{kl} U_k U_l \int_{-\infty}^{\infty} dt \text{Im} \{ [G_{kl}^{<}]^2 [(G_{kl}^{>})^*]^2 \}, \quad (2.123)$$

and thus ΔI is purely imaginary. However, since all reasonable approximations yield real currents, the entire expression vanishes, proving that CPA + 2nd Born is particle conserving.

We should note that current conservation is by no means a trivial fulfillment. It depends crucially on the nature of the self-consistent calculations. As discussed before [52, 54], non-self-consistent approximations (e.g. G_0W_0) are not particle conserving, and in such calculations ΔI can become quite large. We studied ΔI in the first steps in our self-consistent cycle, and found that ΔI could be of the same order as the current itself. However, at self-consistency, we always found that $\Delta I = 0$ to numerical accuracy. This means that self-consistency in CPA is crucial in the case of quantum transport, and care must be taken when considering perturbative treatments.

2. THEORY

3

Numerical methods

To obtain the results in this work, several different codes were used. Some have been written by me, and some has been written by colleagues and co-workers. Three main codes were used: i) A code for exactly solving the Schrödinger equation using the Lanczos algorithm. ii) A DFT and TDDFT code which can compute, for finite or contacted systems, ground-state quantities such as energies and densities, and perform time evolutions to obtain quantities such as time-evolved densities. iii) A many-body code which uses NEGF and calculates ground-state and steady-state properties by solving self-consistently the equations of motion. I wrote the DFT and TDDFT code for finite systems, as well as the NEGF code. Here, the most important aspects of the different codes will be discussed.

3.1 Exact Diagonalization

One of the advantages of using simplified models is that they can often be solved exactly when the size of the system is small. With the commonly used term 'exact', we mean here numerically exact, in turn meaning that we can get the full wavefunction to arbitrary precision. The term 'exact diagonalization' is then to be read as complete, or full, diagonalization. Thus, an exact code can give reliable benchmarks, making it possible to assess the strengths and weaknesses of various approximations. Furthermore, since the wavefunction is obtained, we can calculate all quantities of interest, be they single-particle quantities such as the density, or correlation functions such as the double

3. NUMERICAL METHODS

occupancy $\langle n_\uparrow n_\downarrow \rangle$. This is in contrast to NEGF or TDDFT, where such quantities are not immediate, as discussed before.

In our lattice models, the Hilbert space is finite, meaning that it is possible to enumerate all basis states. One way of constructing the basis states is to use the site basis. Since each lattice site can have four different configurations (empty, occupied by a spin up/down electron, doubly occupied), the space consists of 4^L states. The full space has to be included if we want to study a system which can interchange particles with an environment. In our case, we restrict ourselves to isolated systems at zero temperature, meaning that the state of the system is pure, and we can restrict the Hilbert space to states which have a fixed number of particles. We furthermore consider a Hamiltonian which cannot flip spins, thus making it possible to further restrict the space to fixed numbers of spin-up/spin-down fermions. The space is thus reduced to the number of ways of placing N_\uparrow spin-up fermions and N_\downarrow spin-down fermions on L sites. Instead of 4^L , we have $\binom{L}{N_\uparrow} \binom{L}{N_\downarrow}$ states. If we consider $N_\uparrow = N_\downarrow = 2$ on $L = 8$ sites, the full space is 65536 versus the restricted space of 784, a considerable reduction. Moreover, in lattice systems, the matrices are exceedingly sparse, which means that only the non-zero elements in the Hamiltonian has to be taken into account.

The idea behind the exact diagonalization code is quite simple: i) Find the ground state. ii) Time propagate a chosen initial state (often the ground state) under the influence of an external time-dependent field. We discuss each step below.

3.1.1 Obtaining the ground state

Arguably, the simplest way of obtaining the ground state would be to write down the Hamiltonian in the chosen basis, diagonalizing it to find all the eigenvalues and eigenstates, and then pick out the state with the lowest energy, which will be the ground state (assuming non-degeneracy). This works well for very small systems, but fails for larger systems since the numerical effort for full diagonalization grows cubically with the size of the system. Thus, several methods that can find the ground state without having to find all the eigenvalues and eigenstates exist. The method we have used is the Lanczos method[55], where the original problem is recast into a tri-diagonal one, which is discussed in more detail below.

3.1.2 Details for the time evolution

As in the case of finding the ground state, a straightforward way of doing time evolution would be to, at each time step, approximate the Hamiltonian to be constant at that time interval, and then write

$$|\psi(t + \Delta t)\rangle = e^{-iH(t)\Delta t}|\psi(t)\rangle. \quad (3.1)$$

The problem is then how to obtain the exponential of a matrix. The most obvious way is perhaps to Taylor expand the exponential, but this will result in a non-unitary method. A straightforward way to obtain a unitary time evolution is to diagonalize the Hamiltonian at each time step, $H(t) = Z(t)D(t)Z^\dagger(t)$. Here $Z(t)$ and $D(t)$ are the eigenvectors and eigenvalues of the Hamiltonian at time t . This gives the propagated wavefunction as

$$|\psi(t + \Delta t)\rangle = e^{-iZ(t)D(t)Z^\dagger(t)\Delta t}|\psi(t)\rangle = \quad (3.2)$$

$$= Z(t)e^{-iD(t)\Delta t}Z^\dagger(t)|\psi(t)\rangle \quad (3.3)$$

which is possible to calculate, since the effect of taking the exponential of a diagonal matrix gives the diagonal matrix containing the exponentials of the matrix elements. However, the costly diagonalization has to be done at each time step. Instead, the iterative Lanczos method was used, which is a method that avoids calculating all eigenvalues and eigenstates. New basis states are constructed by applying the Hamiltonian a number of times to a seed state ϕ_0 , giving the set $\{\phi_0, H\phi_0, H^2\phi_0, \dots, H^n\phi_0\}$, the so-called Krylov space.[55] These vectors are then orthogonalized. The Hamiltonian in this new basis, turns out to be tri-diagonal. This is useful, since such matrices can be more efficiently diagonalized. Moreover, because the basis vector n comes from applying H n times to a seed state, it looks very similar to a Taylor expansion, and states with a high n is not as important for short times.[56] Thus, time evolution in this method is always a trade-off between the timestep and the size of the Krylov space. Eq. (3.3) is then used in the subspace. As a final remark, we time-evolve our states using the Hamiltonian at time $t + \Delta t/2$ instead of t , thus gaining an order of accuracy.

In this way, we have time evolved systems which have up to a few million basis states.

3. NUMERICAL METHODS

3.2 TDDFT

This code consists of two parts. First is the part which solves the time-independent Kohn-Sham equations self-consistently, and calculates the ground-state density, ground-state energy and the Kohn-Sham wavefunction (a Slater determinant). The second part performs time evolution, starting from an initial state. We always use the ground state as initial state, but this is by no means necessary.

3.2.1 Solving the time-independent Kohn-Sham equations

We want to solve the time-independent single-particle Kohn-Sham equations, Equation (2.7), in the LDA approximation. The Kohn-Sham equations are

$$\left(\hat{T} + \hat{v}_{KS}\right) \varphi_\nu = \epsilon_\nu \varphi_\nu \quad (3.4)$$

where the Kohn-Sham potential is

$$v_{KS}(i) = v_{ext}(i) + \frac{1}{2}U_i n_i + v_{xc}^{LDA}(n_i). \quad (3.5)$$

The exchange-correlation potential v_{xc} is taken from the corresponding homogeneous reference system. The kinetic energy T is defined from the lattice. As before, the density n is obtained from the occupied orbitals. Thus, these equations have to be solved self-consistently. This was done according to the schematic in Figure 3.1.

3.2.2 Solving the time-dependent Kohn-Sham equations

After the self-consistent loop has been performed, we time evolved the system according to the time-dependent Kohn-Sham equations (2.10). Performing the time evolution can be done in the same way as discussed for the case of exact diagonalization, with one exception. We cannot perform the trick of considering $H(t+\Delta T/2)$ for the time evolution instead of $H(t)$, since $H(t+\Delta t/2)$ depend on the density at time $t+\Delta t/2$. Instead, we performed a simple so-called predictor-corrector scheme: Given $H(t)$, perform the time evolution from t to $t+\Delta t$. Then calculate the effective potential, which gives $H(t+\Delta t)$. Then obtain an approximate Hamiltonian according to $H(t+\Delta t/2) \approx \frac{H(t)+H(t+\Delta t)}{2}$. Do the time evolution again from t to $t+\Delta t$ with $H(t+\Delta t/2)$. This scheme can be repeated as many times as needed, but we found that one iteration is enough for our purposes.

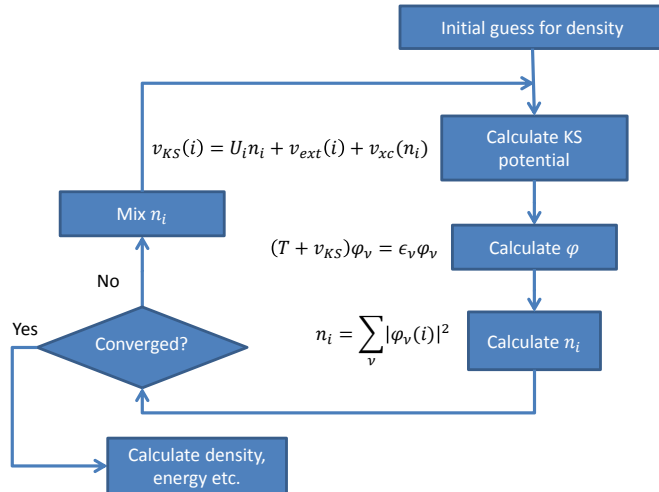


Figure 3.1: Self-consistent iteration scheme of the DFT code. The loop starts with an initial density n_0 , taken e.g. to be constant, or equal to the non-interacting value. The Kohn-Sham potential is constructed, and then the system is diagonalized. The density is obtained from the orbitals, and it is checked whether the new density is equal to the previous one to some accuracy. If not, we restart the loop. For stability, we mix the input density with linear mixing, such that $n_{input} = \alpha n_{new} + (1 - \alpha)n_{previous}$.

For contacted systems using TDDFT, a slightly different algorithm was used. We refer to [57] for details regarding time evolution of open systems.

3.3 NEGF

As stated in the theory section we neglect initial correlations and aim directly at the steady-state. In this case, we only need to choose two independent Green functions. Our choice is $G^R(\omega)$ and $G^<(\omega)$. Other choices are of course possible, such as the combination $G^A, G^>$. One advantage with our choice is that the density is directly obtained from $G^<$. Additionally, in the special case of equilibrium, we can make use of a fluctuation-dissipation theorem[33] to find the lesser Green's function as $G^< = ifA$, that is, directly from the retarded Green's function.

Since we are in equilibrium or in steady state, $G^<$ and G^R depend on $t - t'$ only, and thus we work in ω -space. However, the many-body approximations we use are local in time, but not in frequency where convolutions has do be made. For efficiency, we make use of the Fast Fourier Transform (FFT), specifically, the FFTW-package[58].

3. NUMERICAL METHODS

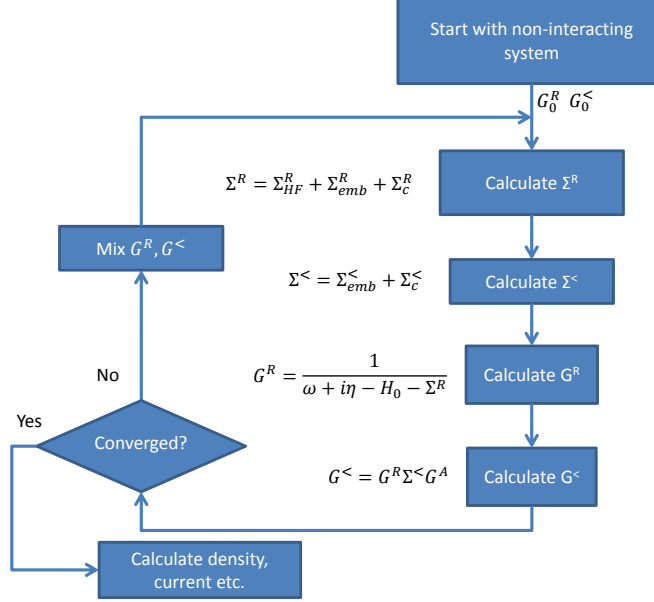


Figure 3.2: Self-consistent iteration scheme of the Green' function code. As the initial guess, we choose the non-interacting Green's function. After this, the Hartree-Fock Green's function is calculated in a separate self-consistent cycle. The resulting Green's function is used as input to the many-body self-consistent cycle. As a test for convergence, we check against the Green's functions themselves.

In a straightforward application of the package, we use an equidistant frequency grid. The grid size $d\omega$ and the maximum/minimum frequency were varied until the result did not depend on the grid itself. The details of the grid depend strongly, of course, on the actual system.

The most computationally intensive parts in the code are: i) Inversion of $G^R(\omega)$, Equation (2.47), which has to be done once per frequency point. ii) FFT for calculating the many-body self-energies. We have cut down the computational effort by utilizing various symmetries, for example $\Sigma^< = -(\Sigma^<)^{\dagger}$. The self-consistent scheme is shown in Figure 3.2.

We have used the code to simulate several different scenarios. In order to treat interactions, we have implemented several different approximations: Hartree-Fock and LDA, as well as 2nd Born. Regarding disorder, we have implemented binary disorder, box disorder, and CPA. The incorporation of the latter is done on the level of adding the self-energies, $\Sigma_c = \Sigma_{MB} + \Sigma_{CPA}$.

3.3.1 Artificial smoothening

Non-interacting, as well as mean-field, calculations can sometimes give rise to energies outside of the band of the leads. Since the self-energy is then purely real, the resulting energies give rise to sharp poles. For numerical convenience, these poles are smoothened, by adding a small imaginary part $\Sigma_{smooth}^R(\omega) = -i\eta$ in the calculation of G^R . This will broaden the poles into Lorentzians of width 2η . Out of equilibrium, this will also change the lesser Green's function according to

$$G^< = G^R (\Sigma_{emb}^< + \Sigma_{smooth}^< + \Sigma_{MB}^<) G^A \quad (3.6)$$

where $(\Sigma_{smooth}^<)_{ij} = 2\eta i f(\omega - \mu) \delta_{ij}$. Thus, the correction to $G^<$ is of the order of η , and will tend to 0 for frequencies where no poles are present. The smoothening can be seen as additional artificial leads in the wide-band limit, where each site is coupled with $\Gamma = 2\eta$ to a separate lead.

Out of equilibrium, currents can leak into the artificial leads, giving the formula for current conservation for a two-probe setup

$$I_L + I_R + \sum_{\alpha} I_{\alpha} = 0, \quad (3.7)$$

where I_{α} is the leakage current into lead α . This leakage current can be calculated from the Meir-Wingreen formula, Eq. (2.66), which can be simplified due to the frequency-independent coupling,

$$I_{\alpha} = 2\eta \int_{-\infty}^{\infty} \frac{d\omega}{2\pi i} (G_{\alpha\alpha}^<(\omega) - 2\pi i f_{\alpha}(\omega) A_{\alpha\alpha}(\omega)) = \quad (3.8)$$

$$= 2\eta n_{\alpha} - 2\eta \int_{-\infty}^{\infty} f_{\alpha}(\omega) A(\omega), \quad (3.9)$$

where n_{α} is the density at site α . Summing over all the leakage currents, and assuming that each lead has the same chemical potential μ , we get

$$\sum_{\alpha} I_{\alpha} = 2\eta N - 2\eta \int_{-\infty}^{\infty} f(\omega - \mu) Tr((A(\omega)), \quad (3.10)$$

where N is the total number of particles in the central region. The smoothening was chosen so that the leakage current was smaller than the real current. One possibility, which we have not implemented yet, is to adjust the chemical potential in each artificial lead at each step in the self-consistency cycle in order to ensure that $I_{\alpha} = 0$.

3. NUMERICAL METHODS

3.3.2 Details for mixing

Solving self-consistent problems is not easy. We have solved them using iterative methods, which does not always need to converge. In order to improve upon the stability, we have frequently been using a linear mixing scheme,

$$X_{in}^{k+1} = \alpha X_{out}^k + (1 - \alpha) X_{in}^k \quad (3.11)$$

X_{in}^k means the input to the self-consistency cycle at the k th iteration, and $X_{out}^k = X_{out}^k[X_{in}^k]$ is the output at iteration k . In the case of DFT, we mix the density, so $X = n$. In the case of NEGF, we mix the Green's functions, so $X = G^R, G^<$. Taking the mixing parameter $\alpha = 1$ removes the mixing, which tends to be unstable in many cases. Small values of α generally means that convergence will be more stable, but slower. Small values such as $\alpha = 0.01$ have been used to converge difficult cases, for instance in the self-consistency cycle in DFT when $v_{xc}(n)$ has a (smoothed) discontinuity. For such cases, we have sometimes changed the mixing parameter during the self-consistency cycle, where we start with a large value, and then gradually decrease it.

Using this simple scheme, it is possible to converge very many of our simulations. However, for the NEGF, we have felt that it was needed to speed up convergence. Several different schemes were tried, and the one which worked the best for us was the Pulay mixing scheme[59], with further refinements from Thygesen and Rubio[52] in order to mix NEGF. In this scheme, one adds history dependence in order to further guess the direction in the self-consistency cycle, by the construction

$$G_{in}^{k+1} = \sum_{n=k-M+1}^k c_n G_{in}^n, \quad (3.12)$$

where M is the number of 'memory terms'. The parameters are chosen so as to minimize the error P , defined to be the residual, $P[G] = G_{out} - G_{in} = G_{out}[G_{in}] - G_{in}$. $P = 0$ means we are at self-consistency. By assuming that the error is linear in G , one obtains

$$P[G_{in}^{k+1}] = \sum_{n=k-M+1}^k c_n P[G_{in}^n]. \quad (3.13)$$

We then minimize the norm of $P[G_{in}^{k+1}]$ with respect to the coefficients c_n . The minimization yields a matrix equation $\mathbf{P}\mathbf{c} = \mathbf{d}$ involving the Pulay residue matrix \mathbf{P} [59],

$$\begin{pmatrix} P_{11} & P_{21} & \cdots & P_{M1} & -1 \\ P_{12} & P_{22} & \cdots & P_{M2} & -1 \\ \vdots & \vdots & \vdots & \ddots & \vdots \\ P_{1M} & P_{2M} & \cdots & P_{MM} & -1 \\ -1 & -1 & \cdots & -1 & 0 \end{pmatrix} \begin{pmatrix} c_1 \\ c_2 \\ \vdots \\ c_M \\ \lambda \end{pmatrix} = \begin{pmatrix} 0 \\ 0 \\ \vdots \\ 0 \\ -1 \end{pmatrix} \quad (3.14)$$

where $P_{kl} = \langle G_{out}^k - G_{in}^k | G_{out}^l - G_{in}^l \rangle$. The last column and row enforces the normalization condition $\sum_n c_n = 1$.

The chosen norm is, as in [52],

$$\langle G_k G_l \rangle = \sum_i \int Im [G_{ii}^k(\omega)] Im [G_{ii}^l(\omega)] d\omega. \quad (3.15)$$

In practice, we solve the matrix equation for G^R only, and then use the same coefficients for the lesser Green function. Also, in the end, we do a linear mixing, giving the final formula

$$G_{in}^{k+1} = \sum_{n=k-M+1}^k c_n [\alpha G_{out}^n + (1 - \alpha) G_{in}^n]. \quad (3.16)$$

Although not implemented in our codes, the same procedure can be used in DFT, by choosing an appropriate norm. Indeed, this is a standard procedure in the DFT community.

3. NUMERICAL METHODS

4

Results

In this section, I summarize the results from the papers, and try to put them in a somewhat larger perspective.

In paper I[46], we study the time evolution of a cloud of fermions in 1D, initially trapped in a parabolic potential. The system is a ring consisting of $L = 100$ lattice sites. This models the situation in cold atoms in optical lattices, where a similar trapping can be used. This system is strongly interacting, having profound effects on the density profile, see Figure 4.1. The parabola tends to keep the fermions in the center, while the interactions tend to push the fermions apart. The result is a competition between these energies, and for intermediate values of the parabola and interaction strengths one obtains a density profile which has several different 'local phases'. We characterize the different parts by their density. The sites which are full, $n = 2$, are part of a local band insulator, while the sites which are half-filled, $n = 1$, are part of a local Mott insulator. Both these parts give rise to characteristic plateaus in the density profile. Away from integer densities, the system has a metallic behavior.

The time evolution of the fermion cloud was studied using lattice TDDFT, which was still a quite new topic at that time. The framework was set up a few years earlier[22], and we used the adiabatic Bethe-Ansatz LDA (BALDA), taken from the 1D homogeneous system. In order to expedite our calculations, we employed an easy-to-use interpolation formula[16]. These types of systems have been studied extensively in ground-state calculations, and motivated by this, we wanted to study aspects related to the time evolution of such systems. One of the interesting aspects is the behavior of the single-site entanglement entropy in time. Ground-state calculations

4. RESULTS

have shown that extrema in the entanglement entropy are indicative of quantum phase transitions[42, 60]. The ground-state entanglement entropy for our system with a trapping potential is shown in Figure 4.1.

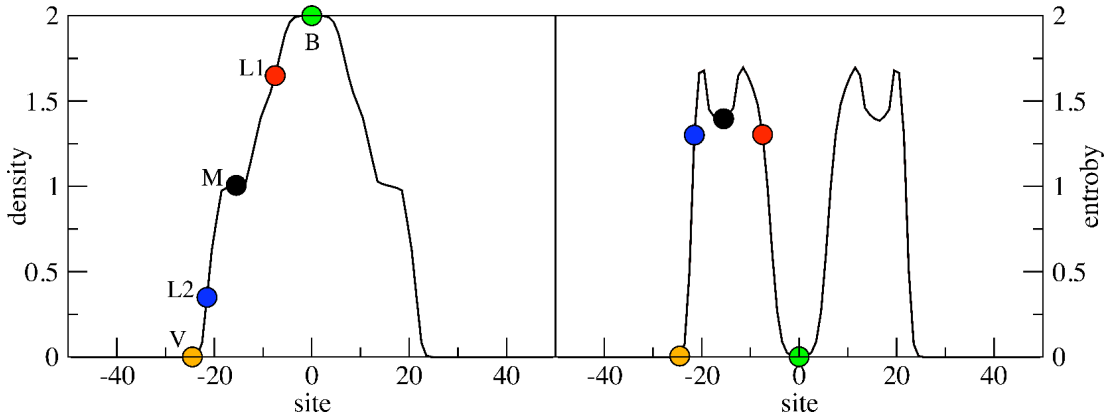


Figure 4.1: Figure from Paper I.[46] Density (left) and entanglement entropy (right) profiles for a chain with $L = 100$ sites and periodic boundary conditions, $N = 60$ fermions with on-site interaction $U = 8$, trapped by a static parabolic potential, $v_{ext} = \frac{1}{2}kx^2$, where the curvature $k = 0.05$. The colored symbols represent sites in the band insulating (B), Luttinger liquid (L1, L2), Mott insulating (M) and near-vacuum (V) regions. In panels b) and c) of Figure 4.2 below, the same colors refer to the same sites.

Using TDDFT, we can evolve for long enough times to be able to achieve the close-to-adiabatic regime. The effect of slowly releasing the trapping potential in time is shown in Figure 4.2. Consistently with previous ground state calculations, we saw that the different parts of the fermion cloud had completely different behavior. The band insulator part melted immediately after the trapping potential was starting to be removed, while the Mott insulator part was stable for a long time. This points to an important difference between the two types of insulators. The same type of behavior was seen for faster removal of the trap, when we are further away from the adiabatic regime. We also saw that the time-dependent entanglement entropy could show information about the local phases of the system.

Having seen the power of TDDFT techniques, being able to simulate quite large strongly interacting systems for long times, we were interested in extending the method to three-dimensional lattices, the subject of Paper II.[61] However, in order to obtain an LDA for inhomogeneous systems, we need to be able to calculate the energy in a homogeneous 3D Hubbard model. As discussed before, no such solution is available

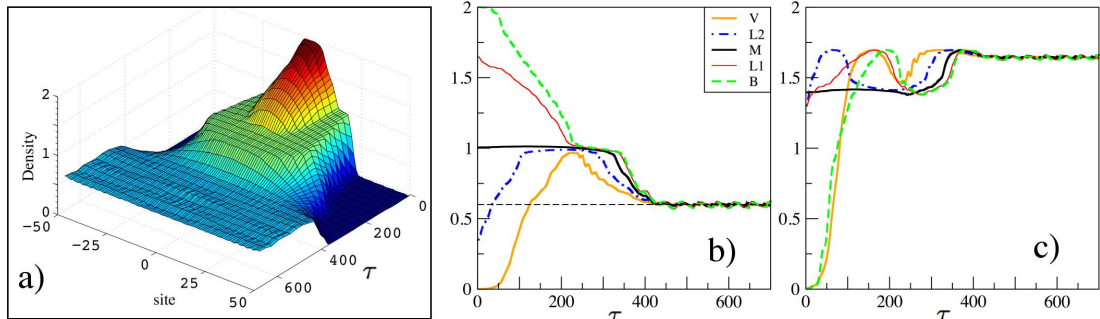


Figure 4.2: Figure from Paper I[46]. Panel a): time-and-space-resolved density profile for adiabatic switching-off of the trapping potential. At time $\tau = 0$ the density profile is that of Figure 4.1, while for later times the curvature of the trap is slowly reduced, allowing the density profile to expand. Panel b): cross-sections of panel a), showing the time evolution of the density at the representative sites indicated in Figure 4.1. The thin horizontal line indicates the uniform density distribution $n_0 (= 0.6)$ for the untrapped system. Panel c): time evolution of the entanglement entropy at the same sites.

in 3D. This system transitions from a metallic phase to an insulating phase if the interaction strength is above a certain critical value[62], which is hard to capture using perturbative methods. Therefore, an approximation, which is non-perturbative in the interaction, was needed.

The method we employed was DMFT (see section 2.3.2), a non-perturbative method shown to be exact in infinite dimensions. Our assumption was that this method could describe well the metal-insulator transition in 3D. Using a DMFT solver, we obtained the exchange-correlation energy E_{xc} by calculating the total energy as a function of density n , and then subtracting the non-interacting kinetic energy and Hartree part,

$$E_{xc}(n) = E_{gs}(n) - T_0(n) - E_H(n). \quad (4.1)$$

The exchange-correlation potential was obtained by taking the derivative, $v_{xc}(n) = \frac{dE_{xc}}{dn}$. We show the results in Figure 4.3. As can be seen, the metal-insulator transition is correctly described, and our v_{xc} will automatically contain this information. Every time the interaction strength is large enough to produce a gap in the DOS, a corresponding discontinuity appears in the exchange-correlation potential.

Having obtained v_{xc}^{DMFT} for the homogeneous system, we obtain an LDA by approximating $v_{xc}[n](i) \approx v_{xc}^{DMFT}(n_i)$, or, for an ALDA, $v_{xc}[n](i, t) \approx v_{xc}^{DMFT}(n_i(t))$. First, we aimed at benchmarking our new v_{xc} , and thus we considered a small enough

4. RESULTS

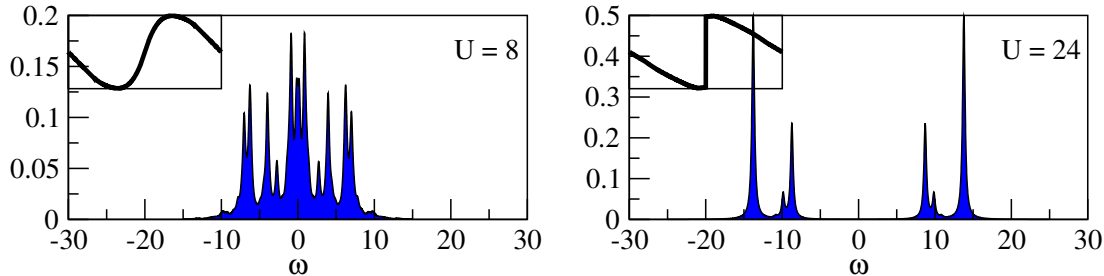


Figure 4.3: Results adopted from Paper II.[61] Density of states at half-filling for interaction strength U below (left) and above (right) the critical value, which will make the system an insulator. For $U = 8$, the spectra is continuous, and the system is a metal. For $U = 24$, a gap has opened, and the system is a (Mott) insulator. In the insets, we show the corresponding v_{xc} as a function of filling. Since DMFT captures the metal-insulator transition, this behavior is automatically captured by our v_{xc} , and manifests as a discontinuity at half-filling density. The density of states is not perfectly smooth because of the finite number of degrees of freedom in the DMFT impurity solver, see 2.3.2.

system to be solved with exact diagonalization. The system considered was a $(5 \times 5 \times 5)$ cluster in 3D, with interaction $U_i = \delta_{ic}U$ only in the center of the cluster. This simplicity was crucial to treat the system, since the high degree of symmetry permitted us to consider a much smaller effective cluster, thus making the exact diagonalization calculations possible. To keep the symmetry also in time, we applied local time-dependent perturbations only to the central site. Note that even if there is interaction only in the center, the exact exchange-correlation potential will generally be non-zero everywhere, since the potential depends non-locally on the density. However, in all ALDA calculations, v_{xc} will be zero at all sites except the central one.

Various perturbing potentials, with different strengths and speeds, were tested against exact calculations. The results are shown in Figure 4.4. Generally, our ALDA could handle both strong and weak interactions. Different perturbations were handled quite well, with the expected behavior that perturbations that were both strong and fast worsened the ALDA results. In one case, however, (strongly interacting, close to half-filling), discrepancies from the exact solutions were found, even in the ground state. To gain insight, we calculated the exact v_{xc} for the ground state (obtainable from knowing the exact density), and saw that non-local effects became very important in this case. Thus, the discrepancy was not due to our ALDA, but the concept of ALDA itself, since non-local contributions needed to be added to the v_{xc} .

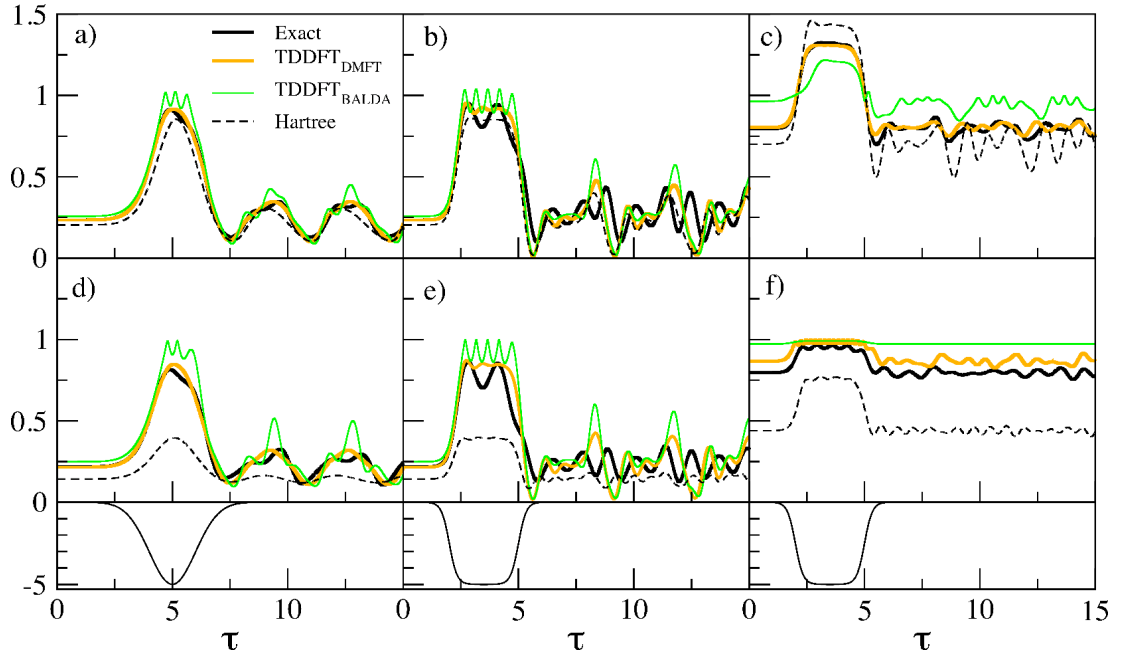


Figure 4.4: Figure from Paper II.[61] Exact, TDDFT, and Hartree density for $U = 8$ (a)–(c) and $U = 24$ (d)–(f) at the central site of a $5 \times 5 \times 5$ cluster with interaction in the center only. In (c) and (f) the cluster has $N_e = 70$ electrons, and $\epsilon_0 = -2.66$ and $\epsilon_0 = -4$, respectively, to attain an initial (and the same) density close to half-filling. Otherwise $N_e = 40$ and $\epsilon_0 = 0$. The time-dependent perturbation $w_0(\tau)$ acts always only at the impurity site, and its shape is shown below (d)–(f). TDDFT-DMFT refers to our ALDA obtained via DMFT. TDDFT-BALDA refers to an ALDA taken from the 1D homogeneous Hubbard model, and is only shown for reference.

The ALDA-DMFT results were generally favorable for a small inhomogeneous cluster. One can assume, based on the nature of the LDA approximation, that studying larger systems will increase the accuracy. Thus, in order to investigate large systems using lattice TDDFT, in Paper IV[63] we decided to study a large inhomogeneous system in 3D, simulating a system relevant in the study of cold atoms in optical lattices. This was to make connections to Paper I, where similar effects were studied in 1D, and also to study the behavior of a large, strongly interacting system. We were also motivated by recent experiments in cold atoms[64]. The setup here was very similar to the 1D calculations in Paper I; we consider a large simple cubic lattice, where a cloud of fermions are initially trapped in a parabolic potential, with $v_{ext} = \frac{1}{2}k(x^2 + y^2 + z^2)$. Again there will be a competition between the interaction energy and the

4. RESULTS

trapping potential, resulting in a density profile which has plateaus of half-filling density - the previously encountered Mott plateaus - resulting in a characteristic 'wedding-cake' structure. We then studied the time evolution of such a system when the trapping potential is removed. Snapshots of the density profile in time are shown in Figure 4.5, which displays results for weak $U = 8$ and for strong $U = 24$ interactions. One can see that the fast switching off of the trapping potential will tend to make the fermion cloud to expand in a symmetrical way, consistent with the underlying cubic lattice. The slower switching-off will tend to keep the spherical shape of the cloud. The density profiles for $U = 8$ is smooth at all times, because the system is metallic, as discussed discussion before. For higher interactions, $U = 24$, the density develops a Mott plateau at half-filling. During the expansion, the band insulator part diminishes immediately, while the Mott plateau is rigid. This is the same behavior as we previously observed in 1D.

A more detailed analysis is shown in Figure 4.6. We found that a useful quantity to study is R_{max} which is outer cloud radius as measured from the center of the system. We found that when the trap was suddenly released, the edge of the cloud expanded ballistically, consistent with previous experiments.[64] The average speed of the cloud, measured with R_{rms} , showed a slower expansion, since this quantity also takes into account the slower core. We could also see that the edge of the Mott plateau never increased in size, as the band insulator melted. This can be seen in Figure 4.6 e), where R_{max} for the Mott region never increased. In previous calculations in 1D[46], we saw an expansion of the width of the Mott plateau, indicating that this phenomena could be an effect of dimensionality. Since the Mott region did not expand, the particle current through the Mott region must be large and constant. Although the current densities would be interesting to study, they can not be obtained rigorously within TDDFT, since the Kohn-Sham current densities themselves have no direct meaning, only the divergence of them, see section 2.5. Even so, we believe that the Kohn-Sham current densities will contain useful information, as long as one is careful about the interpretation of them. The currents are shown in Figure 4.6 f), and one can see that there are indeed quite large currents inside the Mott region, which however keep the density fixed in the Mott plateau.

We also performed simulations comparing a clean lattice to a disordered one; we used the same ground state, and compared how the evolution of the cloud would differ.

The disorder configuration was chosen to be binary disorder, where there are two types of energy levels, randomly spread over the system. In principle, to describe the effects of disorder, we would need to take a large number of these configurations and perform the average over them. However, since this would require a huge effort numerically, we instead picked only one configuration, which was the 'most likely', a so-called quasi-random structure. This structure will generate results close to the averaged ones.[65] The disorder was chosen to be non-zero only beyond the initial cloud radius. We could see that the disorder trapped part of the cloud, since particles could get trapped in lower energies, as well as being reflected off higher energies. Even when the trapping potential was switched off, the particles were trapped mainly in the center of the system. However, there was also another feature visible; the disorder could help the Mott plateau to melt, by opening up additional energetic pathways. Thus, a disordered system could actually melt fast than a homogeneous one. This is an example of the intriguing behavior of the competition between disorder and interactions.

4. RESULTS

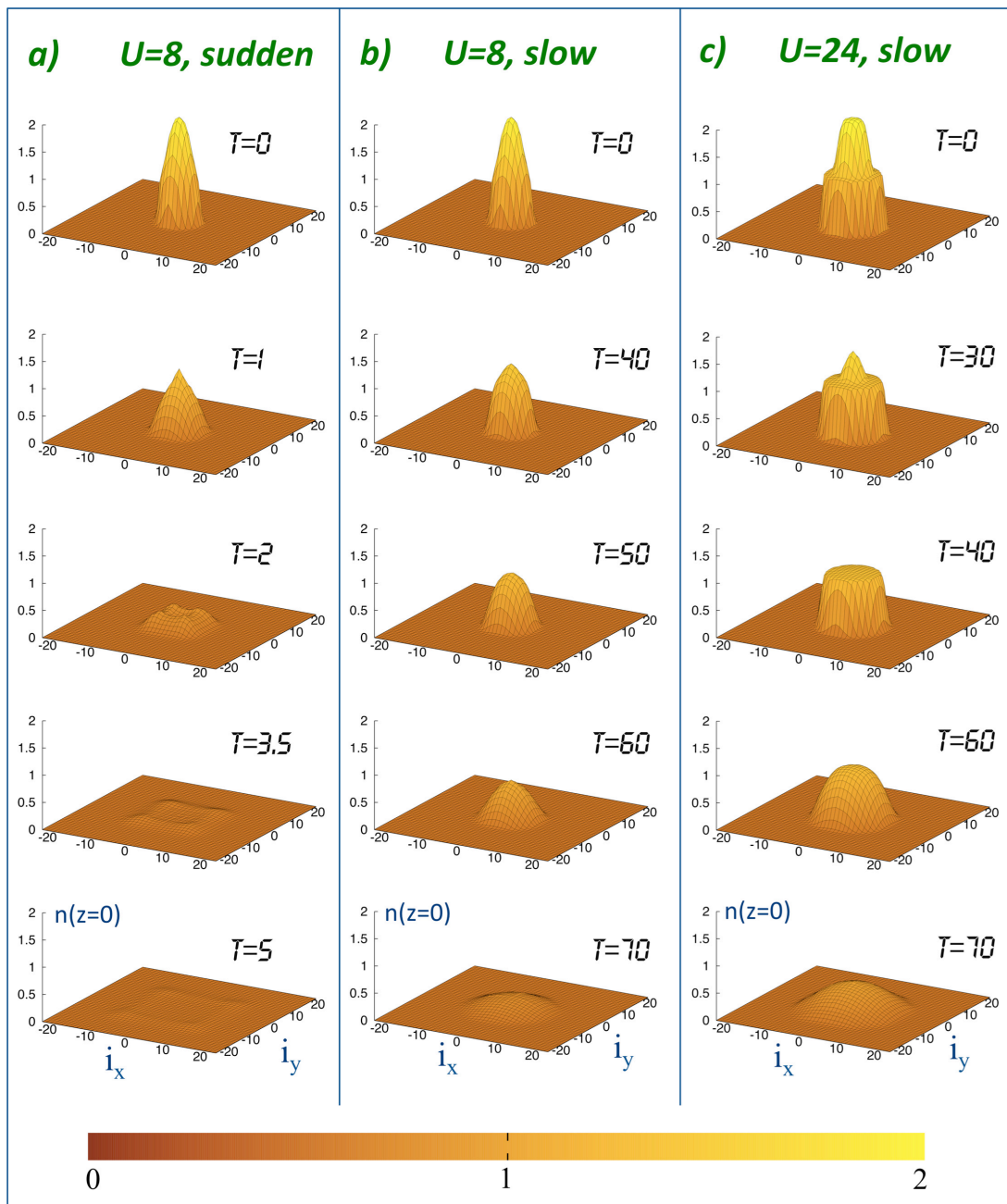


Figure 4.5: Figure from Paper IV.[63] Cloud expansion into a homogeneous lattice. (a), (b), (c): Density profiles in the $x-y$ plane for $z=0$, for different times and setups. The color bar represents the density scale. For the sudden case, the trapping potential is switched off almost immediately. For the slow case, the trap is switched off at $t=80$.

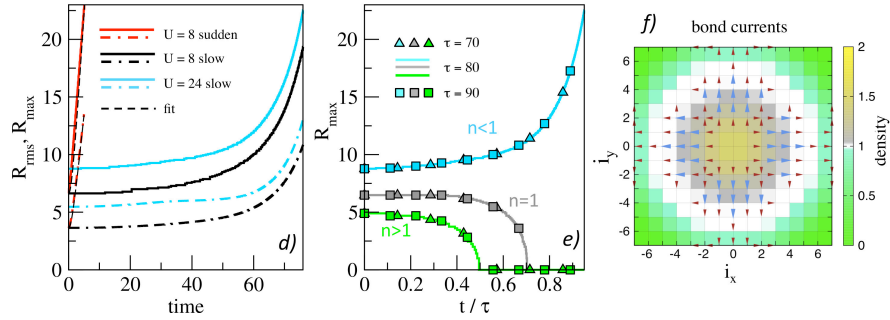


Figure 4.6: Subset of figure from Paper IV.[63] Quantitative analysis of the homogeneous expansion for different times and setups. (d): R_{max} (solid lines) and R_{rms} (dashed-dotted lines). For $U = 8$, sudden expansion, fits are shown (dashed lines). (e): R_{max} for $U = 24$ as a function of rescaled time t/τ . Densities for different trap protocols ($\tau = 70, 80, 90$) have distinct symbols; different density domains have distinct colors. (f): Bond currents and densities in the $z = 0$ plane for $U = 24$, $t = 30$. Blue (red) arrows correspond to large (intermediate) currents, whilst small currents are not shown.

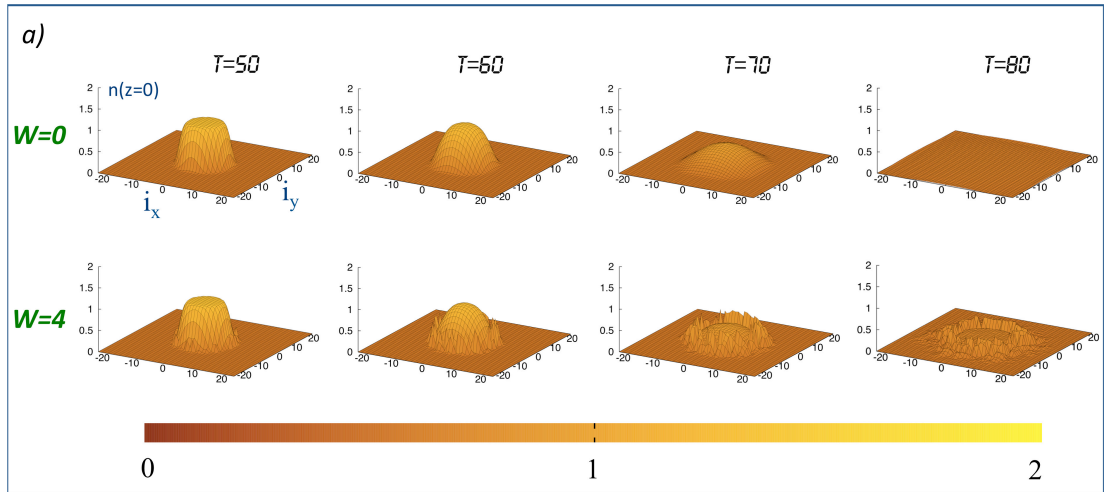


Figure 4.7: Subset of figure from Paper IV.[63] Mott wedding-cake expansion in clean and disordered systems. (a): Comparison between the density profiles in the $z = 0$ plane for the clean, homogeneous case ($W = 0$) (same as in Figure 4.5 c) and the disordered one ($W = 4$).

4. RESULTS

Another highly interesting type of system in which the competition between disorder and interaction plays an important role, is quantum transport geometries. It has been seen that disordered systems, which show an insulating behavior if one assumes a non-interacting picture, are actually conducting. If disorder effects are much stronger than interaction effects, one generally ends up with an insulator of Anderson-type. If the interaction is much stronger than the disorder, one ends up with an insulator of Mott-type. We wanted to see how a system would behave when the disorder and interaction are confined to a finite region, and in a regime away from the limits of only disorder and only interaction. Accordingly, we studied systems consisting of a lead-device-lead geometry, fully one-dimensional, where disorder and interaction effects were present only in the device region. Our device region was a linear chain, while the leads were taken to be infinite in size. We wanted to study the time evolution for such a system, and for this, we made use of TDDFT for contacted systems. This allowed us to study strong values of biases, and transient behavior. However, for low values of U , the interpolation formula widely used in BALDA[16] is not accurate anymore, and thus we resorted to obtain our v_{xc} from the exact solution of the 1D Hubbard model. For more details, see Kartsev[66, 67].

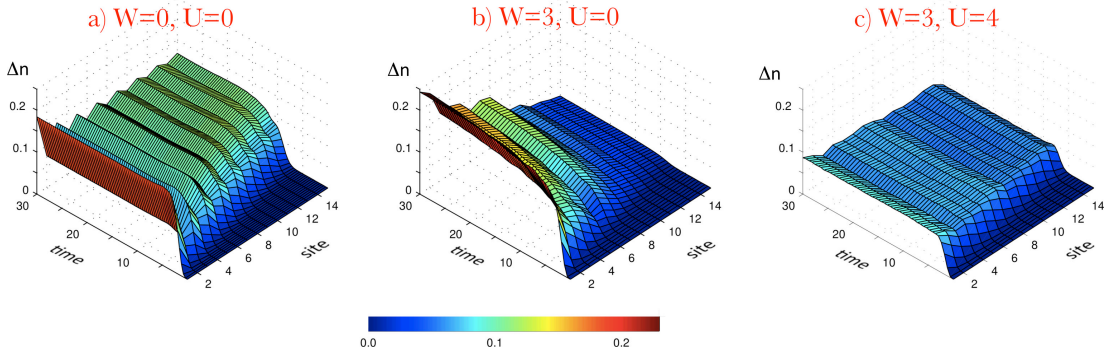


Figure 4.8: Figure from Paper III.[57] Difference between non-equilibrium and ground-state (initial) densities, in a chain with $L = 15, n = 1$, and box disorder W , when a bias $b_S(t)$ is applied in one of the two leads, and $b_0 = 1.5$. The maximum evolution time is $T_{max} = 30$, in units of the inverse hopping parameter in the chain. Arithmetical disorder averaging is performed over 50 configurations.

A relevant question to ask, is how the disorder and interaction will affect the density of such a system. This is shown in Figure 4.8. As one could expect, the density in a non-interacting, homogeneous system (a) is quite smooth, the only irregularity coming

from the finite bias. The addition of strong disorder tend to make the density highly inhomogeneous(b). This is mitigated by the inclusion of interaction effects, which makes the density profile much smoother(c). This can be understood in a mean-field picture, where the effective potential from the electrons tend to smoothen the energy landscape from the disorder. This behavior - a more smooth density as the interaction increases - is quite general, and can be more easily studied using quantities such as the variance of the density, or a closely related quantity, the density Inverse Participation Ratio (IPR), which was also studied in the paper. The usual definition of the IPR was slightly modified in order to study a lead-device- lead geometry. The idea of all IPR measures is to quantify the degree of localization in a system. Our IPR measures the density spread in the device region, meaning that if the density is homogeneous, the density IPR is minimal. It is defined according to

$$dIPR = \frac{\sum_i n_i^2}{(\sum_i n_i)^2}, \quad (4.2)$$

where the sum is restricted to the device region. We found that the density IPR always decreased as a function of interaction, meaning that the density becomes more homogeneous, consistent with Figure 4.8. Thus, we saw that the density IPR and the current showed the same trends.

We also studied the current, as a function of time, for various fillings of the leads and bias strengths, shown in Figure 4.9. We found that increasing disorder would generally decrease the current. Increasing the interaction strength in presence of disorder, however, increases the current through the system. This interesting behavior was seen for all parameters studied.

The lead-device-lead system was studied using TDDFT in the ALDA, which means that our v_{xc} depends locally on the density in the device region only. Moreover, our v_{xc} is zero in the leads. However, it has been seen[68] that the ALDA can overestimate currents in transport calculations. Thus, we wanted to study the same type of system using another approach. We used the NEGF technique, since it allows for inclusion of non-local effects in a systematic way. The geometry of the studied system was very similar, but not exactly the same because of technical reasons. Unfortunately, this means that we can not compare the TDDFT results with those from the NEGF quantitatively. Instead, we will focus on the qualitative differences and similarities.

4. RESULTS

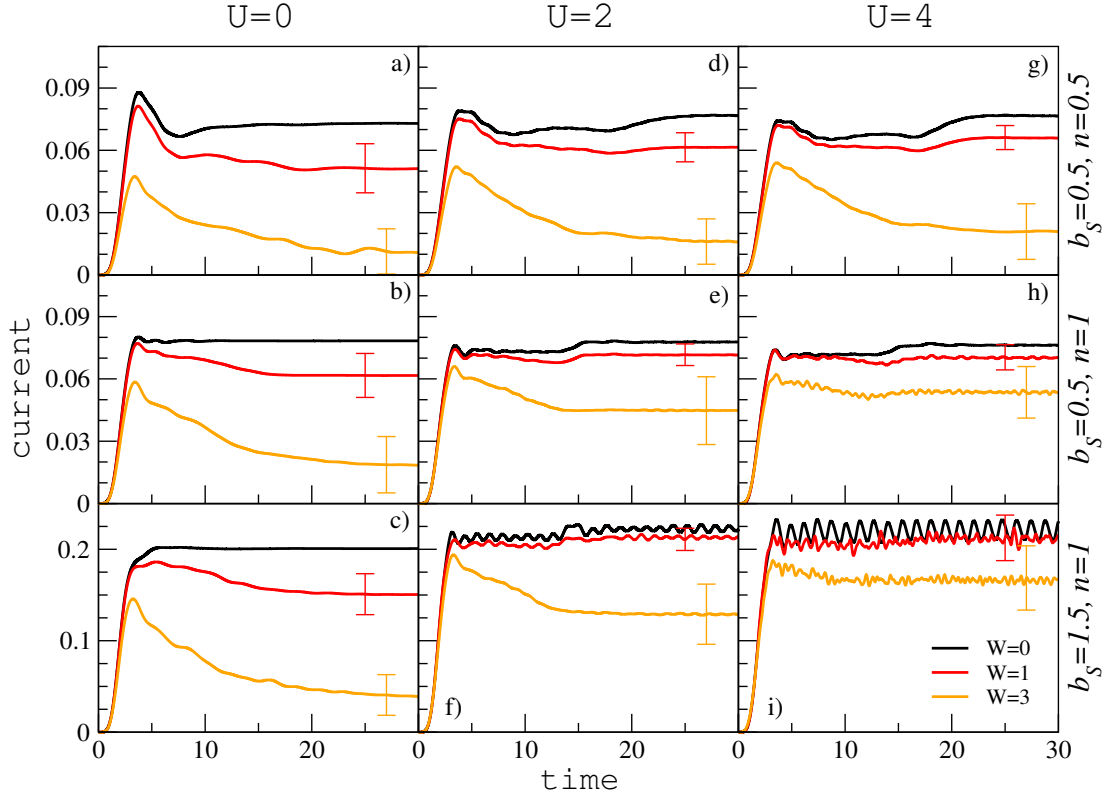


Figure 4.9: Figure from Paper III.[57] Time-dependent average currents as function of time for a chain with $L = 15$ sites, and different interactions strengths ($U = 0, 2, 4$). The currents shown are computed at the leftmost bond in the chain. The bias b_S and the band filling n for panels in the same row are specified on the right, while in each panel, the current is displayed for three disorder strengths ($W = 0, 1, 3$). The configuration averages were obtained from 50 instances of box disorder. For $W > 0$, the inherent standard deviations in the long-time limit are shown as vertical bars.

We studied systems up to $L = 20$, and we study directly the steady-state behavior without time evolutions. We found that many of the results were similar to the ones obtained via TDDFT in Paper III, but there was an important difference. The similarities were that the density became more smooth as the interaction was increased, and currents could increase in a disordered system, when interactions were included. However, we found that this was not always the case. Instead, we found a non-monotonic behavior in the current. Starting from a disordered system, the interaction first increases the current, but after reaching a maximum at $U \approx W$, the current goes down again. This is shown in Figure 4.10. The same behavior could be seen for differential

conductances $\sigma = \frac{dI}{db_L}$. For more results, including finite-size scalings of conductances and entanglement entropy, we refer the reader to Paper V[53].

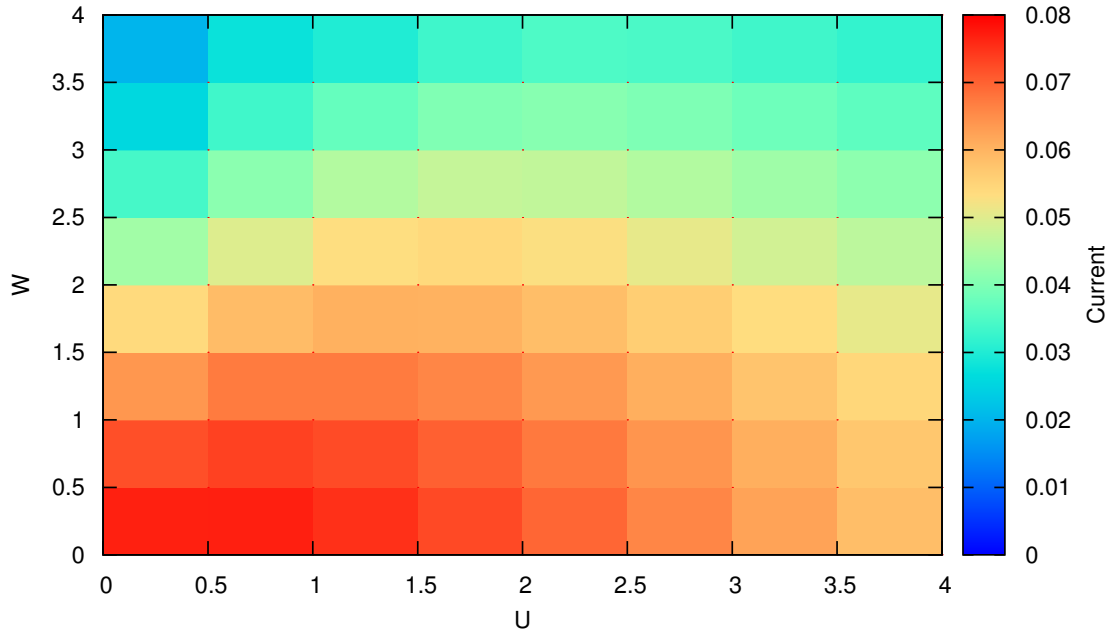


Figure 4.10: Figure from Paper V[53]. Current for bias $b_L = 0.5$ as a function of interaction and disorder. All calculations are done using box disorder, and we show the averaged currents. Keeping the value of interaction fixed, the current is decreased if disorder is increased. However, fixing the disorder strength, we see a non-monotonous behavior in the current, where the maximum of the current seems to be around $U \approx W$. [53]

4. RESULTS

5

Conclusions and Outlook

The aim of this thesis has been to study strongly correlated systems by using and improving existing methods and by developing new ones.

It is often difficult to know a priori whether a certain approach is suitable to a specific problem. Accordingly, a large part of my work has been to assess approximations, most often by studying very simple systems where comparisons with the exact solution is possible. We have found that such benchmarking is highly valuable in order to see the strengths and weaknesses of different approaches. In some cases it has been difficult to find suitable benchmark systems. In these cases, we have found that insight can be gained from comparing different approximations.

One of the main outcomes from our work is the construction of a class of approximate exchange-correlation potentials usable for lattice systems in three dimensions.[61] They are based on the solution of a homogeneous reference system, obtained using DMFT. Descriptions of inhomogeneous systems using DFT or TDDFT can be approximated by using these new potentials. In ground-state calculations, the potentials can be used as an LDA, while in the time-dependent case they can be used as an ALDA. The potentials are applicable both for weakly and for strongly interacting systems. Benchmarks against exact calculations have shown that the approximate potentials give results that compare well in many cases, even when a moderately strong and moderately fast time-dependent external field is applied to the system. We have found cases where our ALDA gives unsatisfactory results. However, we have proved, via construction of the exact exchange-correlation potential, that it is not our way of obtaining the ALDA via DMFT that fails. Instead, we have attributed the shortcomings to the

5. CONCLUSIONS AND OUTLOOK

breakdown of the ALDA itself. Thus, it seems that our ALDA is an efficient, non-perturbative approximation, which could be useful for studying the time evolution of large three-dimensional inhomogeneous systems.

Using this new ALDA, we have shown[63] that it is possible to study the time evolution of thousands of strongly interacting particles. We have performed simulations that involved hundreds of thousands of lattice sites - large enough to be relevant for experimental conditions. This allowed us to study the difference between band insulators and Mott insulators. We found that Mott plateaus are very stable against changes in the external potential, whereas band insulating regions are not. The same time-dependent behavior has been found in one dimension.[46]

Even though the exchange-correlation potentials obtained via DMFT has been shown to perform well in many cases, it is not trivial to construct them. The potentials has to be obtained for the entire density range. Moreover, the potential has to be tailored to each specific situation. Thus, in order to compare lattice TDDFT to experiments, we would need to obtain new exchange-correlation potentials for each set of experimental parameters. Thus, we would like to develop a more expedient way of constructing the potentials. Inspiration could come from the one-dimensional case. There, interpolation formulas that obey known exact results in certain limits have been constructed.[16] In three dimensions, the number of exact results are fewer. Moreover, in contrast to from the one-dimensional case, the Mott-Hubbard insulator transition in three dimensions occurs at a finite value of U , making it more difficult to find a general interpolation formula which is accurate both for weakly and strongly interacting systems.

Another aspect of this work concerns the behavior of systems where strongly interacting particles reside in a disordered landscape. It has been known for quite some time that disordered systems in general have a very poor conductivity[69]. In the thermodynamical limit, a three-dimensional system becomes insulating at a finite value of the disorder strength, while for smaller dimensions any disorder is enough to induce an insulating behavior. An inhibited conductivity is also observed for strongly interacting systems. For strong enough interactions, the system transforms into a Mott insulator. However, when strong interaction and disorder effects are considered simultaneously, the two effects compete against each other, changing the behavior of the system. For

systems away from the thermodynamical limit, where finite size effects complicates the picture, less work has been done. We have studied the competition between disorder and interaction in short chains contacted to leads, using TDDFT[57] and using NEGF[53].

Our studies concluded that disorder enhances localization in short chains, decreasing the current through the junction as compared to a non-disordered chain. However, adding strong interactions to the chain can make it more conducting, since interparticle interactions tend to delocalize particles. This is consistent with experimental results, performed on 2D Silicon-MOSFET samples.[70, 71, 72, 73, 74] Using TDDFT, we found that an increase of the interaction strength always tended to increase the current through the system. We saw the same type of increase in many cases also using NEGF. However, when the interaction was increased further, we saw a decrease in the current.

The trend seen using NEGF is consistent with previous studies.[75] Since this trend is not seen in our TDDFT calculations, we must attribute this to our only approximation, the ALDA. It is still an open question under which conditions it is enough to consider an exchange-correlation potential in the interacting device region only. In some cases, [76, 77], it has been shown that the real exchange-correlation potential extends far into the leads. It has also been shown[68] that using ALDA for such systems can produce reliable densities, but tend to overestimate currents. This would suggest that non-local effects are important for a reliable description. Such effects are automatically included in the NEGF formalism. However, the non-perturbative nature of TDDFT makes it an extremely computationally inexpensive method that has proven to produce reliable results in many scenarios. Because of the complementary strengths and weaknesses of the different methods, further developments in parallel of the two approaches could help in unravelling the physics of strongly correlated systems.

5. CONCLUSIONS AND OUTLOOK

References

- [1] J. HUBBARD. **Electron correlations in narrow energy bands.** *Proceedings of the Royal Society of London*, **276**(1365):238–257, 1963. 5
- [2] F. H. L. ESSLER, H. FRAHM, F. GÖHMANN, A. KLÜMPER, AND V. E. KOREPIN. *The One-Dimensional Hubbard model.* Cambridge University Press, 2005. 7
- [3] I. BLOCH AND W. ZWERGER. **Many-body physics with ultracold gases.** *Reviews of Modern Physics*, **80**(3):885–964, July 2008. 7
- [4] E. H. LIEB AND F. Y. WU. **Absence of Mott transition in an exact solution of the short-range, one-band model in one dimension.** *Physical Review Letters*, 1968. 7, 12, 13
- [5] W. METZNER AND D. VOLLHARDT. **Correlated lattice fermions in $d=\infty$ dimensions.** *Physical review letters*, **62**(3), 1989. 7, 14, 15
- [6] K. CAPELLE AND V. L. CAMPO. **Density functionals and model Hamiltonians: Pillars of many-particle physics.** *Physics Reports*, **528**(3):91–159, July 2013. 8, 13
- [7] U. VON BARTH. **Basic Density-Functional Theory—an Overview.** *Physica Scripta*, pages 9–39, 2006. 8
- [8] P. HOHENBERG AND W. KOHN. **Inhomogeneous electron gas.** *Physical Review*, **155**(1962), 1964. 8
- [9] M. LEVY. **Universal variational functionals of electron densities, first-order density matrices, and natural spin-orbitals and solution of the v -representability problem.** *Proceedings of the National Academy of Sciences*, **76**(12):6062–6065, 1979. 8

REFERENCES

- [10] W. KOHN AND L. J. SHAM. **Self-consistent equations including exchange and correlation effects.** *Physical review*, **140**(4A), 1965. 10
- [11] E. RUNGE AND E. K. U. GROSS. **Density-functional theory for time-dependent systems.** *Physical Review Letters*, **52**(12), 1984. 11
- [12] R. VAN LEEUWEN. **Mapping from Densities to Potentials in Time-Dependent Density-Functional Theory.** *Physical Review Letters*, **82**(19):3863–3866, May 1999. 11
- [13] O. GUNNARSSON AND K. SCHÖNHAMMER. **Density-functional treatment of an exactly solvable semiconductor model.** *Physical review letters*, **56**(18), 1986. 12
- [14] K. SCHÖNHAMMER AND O. GUNNARSSON. **Discontinuity of the exchange-correlation potential in density functional theory.** *Journal of Physics C: Solid State Physics*, **3675**(20), 1987. 12
- [15] K. SCHÖNHAMMER, O. GUNNARSSON, AND R. M. NOACK. **Density-functional theory on a lattice: Comparison with exact numerical results for a model with strongly correlated electrons.** *Physical Review B*, **52**(4), 1995. 12
- [16] N. A. LIMA, M. F. SILVA, L. N. OLIVEIRA, AND K. CAPELLE. **Density functionals not based on the electron gas: Local-density approximation for a luttinger liquid.** *Physical Review Letters*, **90**(14):146402, 2003. 13, 27, 47, 56, 62
- [17] N. A. LIMA, L. N. OLIVEIRA, AND K. CAPELLE. **Density-functional study of the Mott gap in the Hubbard model.** *EPL (Europhysics Letters)*, **601**, 2002. 13
- [18] M. SILVA, N. LIMA, A. MALVEZZI, AND K. CAPELLE. **Effects of nanoscale spatial inhomogeneity in strongly correlated systems.** *Physical Review B*, **71**(12):125130, March 2005. 13

-
- [19] G. XIANLONG, M. POLINI, M. TOSI, V. L. CAMPO, K. CAPELLE, AND M. RIGOL. **Bethe ansatz density-functional theory of ultracold repulsive fermions in one-dimensional optical lattices.** *Physical Review B*, **73**(16):165120, April 2006. 13
- [20] V. FRANÇA AND K. CAPELLE. **Entanglement in Spatially Inhomogeneous Many-Fermion Systems.** *Physical Review Letters*, **100**(7):070403, February 2008. 13, 27
- [21] V. V. FRANÇA, D. VIEIRA, AND K. CAPELLE. **Simple parameterization for the ground-state energy of the infinite Hubbard chain incorporating Mott physics, spin-dependent phenomena and spatial inhomogeneity.** *New Journal of Physics*, **14**(7):073021, July 2012. 13
- [22] C. VERDOZZI. **Time-Dependent Density-Functional Theory and Strongly Correlated Systems : Insight from Numerical Studies.** *Physical Review Letters*, **101**(16):166401, 2008. 13, 47
- [23] R. BAER. **On the mapping of time-dependent densities onto potentials in quantum mechanics.** *The Journal of chemical physics*, **128**(4):044103, January 2008. 13
- [24] M. FARZANEHPUR AND I. TOKATLY. **Time-dependent density functional theory on a lattice.** *Physical Review B*, **86**(12):125130, September 2012. 13
- [25] C. FIOLHAIS, F. NOGUEIRA, AND M. A. L. MARQUES, editors. *A Primer in Density Functional Theory*, **620** of *Lecture Notes in Physics*. Springer Berlin Heidelberg, Berlin, Heidelberg, June 2003. 13
- [26] M. A.L. MARQUES, N. T. MAITRA, F. M. S. NOGUEIRA, E. K. U. GROSS, AND A. RUBIO, editors. *Fundamentals of Time-Dependent Density Functional Theory*, **837** of *Lecture Notes in Physics*. Springer Berlin Heidelberg, Berlin, Heidelberg, 2012. 13
- [27] CARSTEN A. ULLRICH. *Time-Dependent Density-Functional Theory: Concepts and Applications*. Oxford University Press, 2012. 13

REFERENCES

- [28] C. VERDOZZI, D. KARLSSON, M. PUIG VON FRIESEN, C.-O. ALMBLADH, AND U. VON BARTH. **Some open questions in TDDFT: Clues from lattice models and Kadanoff–Baym dynamics.** *Chemical Physics*, **391**(1):37–49, November 2011. 13
- [29] A. GEORGES AND G. KOTLIAR. **Hubbard model in infinite dimensions.** *Physical Review B*, **45**(12), 1992. 14
- [30] A. GEORGES, G. KOTLIAR, W. KRAUTH, AND M. J. ROZENBERG. **Dynamical mean-field theory of strongly correlated fermion systems and the limit of infinite dimensions.** *Reviews of Modern Physics*, **68**(1), 1996. 15
- [31] G. KOTLIAR AND D. VOLLHARDT. **Strongly correlated materials: Insights from dynamical mean-field theory.** *Physics Today*, **57**(3):53–59, 2004. 15
- [32] A. L. FETTER AND J. D. WALECKA. *Quantum Theory of Many-Particle Theory.* Dover Publications, 2003. 16
- [33] G. STEFANUCCI AND R. VAN LEEUWEN. *Nonequilibrium Many-Body Theory of Quantum Systems: A Modern Introduction*, **54**. Cambridge University Press, July 2013. 18, 23, 41
- [34] Y. ZHU, L. LIU, AND H. GUO. **Quantum transport theory with nonequilibrium coherent potentials.** *Physical Review B*, **88**(20):205415, November 2013. 21, 33
- [35] M. HOPJAN. *Nonequilibrium superconductivity.* PhD thesis, 2012. 21
- [36] J. R. HELLUMS AND W. R. FRENSLEY. **Non-Markovian open-system boundary conditions for the time-dependent Schrödinger equation.** *Physical Review B*, **49**(4):2904–2906, 1994. 22
- [37] S. KURTH, G. STEFANUCCI, C.-O. ALMBLADH, A. RUBIO, AND E. K. U. GROSS. **Time-dependent quantum transport: A practical scheme using density functional theory.** *Physical Review B*, **72**(3):1–13, July 2005. 22
- [38] P. MYÖHÄNEN. *Many-Particle Theory for Time-Dependent Quantum Transport in Nanostructures.* PhD thesis, University of Jyväskylä, 2012. 23

-
- [39] Y. MEIR AND N. S. WINGREEN. **Landauer formula for the current through an interacting electron region.** *Physical review letters*, **68**(16):2512, 1992. 24
- [40] M. PUIG VON FRIESEN, C. VERDOZZI, AND C.-O. ALMBLADH. **Can we always get the entanglement entropy from the Kadanoff-Baym equations? The case of the T-matrix approximation.** *EPL (Europhysics Letters)*, **95**(2):27005, July 2011. 25
- [41] S. J. GU, S. S. DENG, Y. Q. LI, AND H. Q. LIN. **Entanglement and quantum phase transition in the extended Hubbard model.** *Physical review letters*, (August):1–4, 2004. 25
- [42] D. LARSSON AND H. JOHANNESSON. **Single-site entanglement of fermions at a quantum phase transition.** *Physical Review A*, pages 2–5, 2006. 25, 48
- [43] C.-O. ALMBLADH AND U. VON BARTH. **Exact results for the charge and spin densities, exchange-correlation potentials, and density-functional eigenvalues.** *Physical Review B*, **31**(6):3231–3244, 1985. 26
- [44] H. MERA AND Y. M. NIQUET. **Are Kohn-Sham Conductances Accurate?** *Physical Review Letters*, **105**(21):216408, November 2010. 26
- [45] H. MERA, K. KAASBJERG, Y. M. NIQUET, AND G. STEFANUCCI. **Assessing the accuracy of Kohn-Sham conductances using the Friedel sum rule.** *Physical Review B*, **81**(3):035110, January 2010. 26
- [46] D. KARLSSON, C. VERDOZZI, M. M. ODASHIMA, AND K. CAPELLE. **Dynamical self-stabilization of the Mott insulator: Time evolution of the density and entanglement entropy of out-of-equilibrium cold fermion gases.** *EPL (Europhysics Letters)*, **93**(2):23003, January 2011. 27, 47, 48, 49, 52, 62
- [47] D. A. ROWLANDS. **Short-range correlations in disordered systems: non-local coherent-potential approximation.** *Reports on Progress in Physics*, **72**(8):086501, August 2009. 30
- [48] E. N. ECONOMOU. *Green's functions in quantum physics*. Springer Berlin Heidelberg, third edition, 2006. 31

REFERENCES

- [49] P. SOVEN. **Coherent-potential model of substitutional disordered alloys.** *Physical Review*, **156**(3), 1967. 32
- [50] K. CARVA, I. TUREK, J. KUDRNOVSKÝ, AND O. BENGONE. **Disordered magnetic multilayers: Electron transport within the coherent potential approximation.** *Physical Review B*, **73**(14):144421, April 2006. 33
- [51] Y. KE, K. XIA, AND H. GUO. **Disorder Scattering in Magnetic Tunnel Junctions: Theory of Nonequilibrium Vertex Correction.** *Physical Review Letters*, **100**(16):166805, April 2008. 33
- [52] K. THYGESEN AND A. RUBIO. **Conserving GW scheme for nonequilibrium quantum transport in molecular contacts.** *Physical Review B*, **77**(11):115333, March 2008. 34, 35, 44, 45
- [53] D. KARLSSON AND C. VERDOZZI. **Transport of correlated electrons through disordered chains.** *arXiv:*, 2014. 34, 59, 63
- [54] A. STAN, N. E. DAHLEN, AND R. VAN LEEUWEN. **Time propagation of the Kadanoff-Baym equations for inhomogeneous systems.** *The Journal of chemical physics*, **130**(22):224101, June 2009. 35
- [55] C. LANCZOS. **An iteration method for the solution of the eigenvalue problem of linear differential and integral operators.** *J. Res. Natl. Bur. Stand.*, **4**(255), 1950. 38, 39
- [56] D. J. TANNOR. *Introduction to Quantum Mechanics: A Time-Dependent Perspective.* University Science Books, 2007. 39
- [57] V. VETTCHINKINA, A. KARTSEV, D. KARLSSON, AND C. VERDOZZI. **Interacting fermions in one-dimensional disordered lattices: Exploring localization and transport properties with lattice density-functional theories.** *Physical Review B*, **87**(11):115117, March 2013. 41, 56, 58, 63
- [58] M. FRIGO. **A fast Fourier transform compiler.** *ACM SIGPLAN Notices*, **34**(5):169–180, May 1999. 41

-
- [59] P. PULAY. **Convergence acceleration of iterative sequences. The case of SCF iteration.** *Chemical Physics Letters*, **73**(2), 1980. 44, 45
- [60] V. V. FRANÇA AND K. CAPELLE. **Entanglement of strongly interacting low-dimensional fermions in metallic, superfluid, and antiferromagnetic insulating systems.** *Physical Review A*, pages 17–19, 2006. 48
- [61] D. KARLSSON, A. PRIVITERA, AND C. VERDOZZI. **Time-Dependent Density-Functional Theory Meets Dynamical Mean-Field Theory: Real-Time Dynamics for the 3D Hubbard Model.** *Physical Review Letters*, **106**(11):116401, March 2011. 48, 50, 51, 61
- [62] F. MANCINI. **The Mott-Hubbard transition and the paramagnetic insulating state in the two-dimensional Hubbard model.** *EPL (Europhysics Letters)*, **229**, 2000. 49
- [63] A. KARTSEV, D. KARLSSON, A. PRIVITERA, AND C. VERDOZZI. **Three-dimensional dynamics of a fermionic Mott wedding-cake in clean and disordered optical lattices.** *Scientific Reports*, **3**(2570):1–7, September 2013. 51, 54, 55, 62
- [64] U. SCHNEIDER, L. HACKERMÜLLER, J. P. RONZHEIMER, S. WILL, S. BRAUN, T. BEST, I. BLOCH, E. DEMLER, S. MANDT, D. RASCH, AND A. ROSCH. **Fermionic transport and out-of-equilibrium dynamics in a homogeneous Hubbard model with ultracold atoms.** *Nature Physics*, **8**(3):213–218, January 2012. 51, 52
- [65] A. ZUNGER, S.-H. WEI, L. G. FERREIRA, AND J. E. BERNARD. **Special quasirandom structures.** *Physical Review Letters*, **65**(3):353–356, 1990. 53
- [66] A. KARTSEV. *Non-equilibrium fermions within lattice density functional theory: quantum transport and ultracold-atom phenomena.* PhD thesis, Lund University, 2013. 56
- [67] A. KARTSEV. **Lattice Density Functional Theory for Cold Atoms and Quantum Transport.** *unpublished*, 2014. 56

REFERENCES

- [68] A.-M. UIMONEN, E. KHOSRAVI, A. STAN, G. STEFANUCCI, S. KURTH, R. VAN LEEUWEN, AND E. K. U. GROSS. **Comparative study of many-body perturbation theory and time-dependent density functional theory in the out-of-equilibrium Anderson model.** *Physical Review B*, **84**(11):28–32, September 2011. 57, 63
- [69] P. W. ANDERSON. **Absence of diffusion in certain random lattices.** *Physical review*, **109**(5), 1958. 62
- [70] T. N. ZAVARITSKAYA AND E. I. ZAVARITSKAYA. **Metal-insulator transition in inversion channels of silicon MOS structures.** *JETP Lett*, **45**(10):476–480, 1987. 63
- [71] S. V. KRAVCHENKO, G. V. KRAVCHENKO, J. E. FURNEAUX, V. M. PUDALOV, AND M. D’IORIO. **Possible metal-insulator transition at $B=0$ in two dimensions.** *Physical Review B*, **50**(11), 1994. 63
- [72] S. V. KRAVCHENKO, W. E. MASON, G. E. BOWKER, J. E. FURNEAUX, V. M. PUDALOV, AND M. D’IORIO. **Scaling of an anomalous metal-insulator transition in a two-dimensional system in silicon at $B=0$.** *Physical Review B*, **51**(11), 1995. 63
- [73] S. V. KRAVCHENKO, D. SIMONIAN, M. P SARACHIK, W. MASON, AND J. E. FURNEAUX. **Electric Field Scaling at a $B=0$ Metal-Insulator Transition in Two Dimensions.** *Physical review letters*, **77**(24):4938–4941, December 1996. 63
- [74] D. POPOVIĆ, A. B. FOWLER, AND S. WASHBURN. **Metal-insulator transition in two dimensions: Effects of disorder and magnetic field.** *Physical review letters*, **79**(8):1543–1546, 1997. 63
- [75] J. WERNSDORFER, G. HARDER, U. SCHOLLWOCK, AND W. HOFSTETTER. **Signatures of Delocalization in the Fermionic 1D Hubbard Model with Box Disorder: Comparative Study with DMRG and R-DMFT.** pages 1–8, August 2011. 63

- [76] S. KURTH AND G. STEFANUCCI. **Dynamical Correction to Linear Kohn-Sham Conductances from Static Density Functional Theory.** *Physical Review Letters*, **111**(3):030601, July 2013. 63
- [77] P. SCHMITTECKERT, M. DZIERZAWA, AND P. SCHWAB. **Exact time-dependent density functional theory for impurity models.** *Physical chemistry chemical physics : PCCP*, **15**(15):5477–81, April 2013. 63